

TECHNICAL REPORT 1921  
October 2003

# **Film Implementation of a Neutron Detector (FIND): Proof of Concept Device**

W. C. McGinnis

Approved for public release;  
distribution is unlimited.

SSC San Diego



TECHNICAL REPORT 1921  
October 2003

# Film Implementation of a Neutron Detector (FIND): Proof of Concept Device

W. C. McGinnis

Approved for public release;  
distribution is unlimited.



*SPAWAR  
Systems Center  
San Diego*

SSC San Diego  
San Diego, CA 92152-5001

## **ACKNOWLEDGMENTS**

The author gratefully acknowledges the supporting contribution of the FIND project sponsor, the Defense Threat Reduction Agency (DTRA), for the period of performance from April 2002 through September 2003 at a funding level of \$300K. The assistance and guidance of program manager Dexter Simmons and supervisor LTC Thomas Cartledge at DTRA are greatly appreciated.

The author also thanks the individuals at the following institutions for their dedicated efforts on the project (see contributions listed under PROJECT PERSONNEL):

### **University of Michigan:**

- Dr. Roy Clarke (professor and director of the Applied Physics Program)
- Pedro Encarnación (graduate research assistant)
- Abishai Daniel (graduate research assistant)

### **Virginia Commonwealth University:**

- Dr. Gary Tepper (associate professor in the Department of Mechanical Engineering)
- Dr. Royal Kessick (post-doctoral student)

### **SPAWAR Systems Center, San Diego:**

- Jennifer Beyer (graduate student contractor from San Diego State University)
- Dr. Manjit Randhawa (visiting professor from Southern University, Baton Rouge)
- Dr. Jon Losee (SSC San Diego Code 2741)
- Ron Brockus (SSC San Diego Code 2741)
- Ed Wesley (SSC San Diego Code 2741)



# EXECUTIVE SUMMARY

## OBJECTIVE

This research and development effort, Film Implementation of a Neutron Detector (FIND), serves as proof of concept for a new type of solid-state neutron detector technology, potentially providing improvements in sensitivity, size, weight, power consumption, operator safety, transportability, and cost compared to current neutron detector technology. The aim of the FIND project is to demonstrate the detection of thermal neutrons with a solid-state device based on boron nitride (BN) films.

## RESULTS

A proof-of-concept FIND device, with a thin bulk BN detecting element, has been successfully demonstrated to be sensitive to irradiation by thermal neutrons. The required material properties for a BN detecting element and its electrical contacts have been defined and investigated in thin film and bulk samples of hexagonal-phase boron nitride. Various characterization methods have been examined for measuring the critical properties of a number of BN samples, including:

- Microwave cavity perturbation (carrier lifetime)
- Time-resolved reflectivity (carrier lifetime)
- Constant-current corona-discharge-induced surface potential build-up (carrier mobility)
- Transmission line method (contact resistance)

## RECOMMENDATIONS

The successful operation of a bulk BN thermal neutron detector affirms the basic concept of the FIND device. Further work is needed to make a reproducible and reliable detector, and to incorporate and optimize a high-quality BN film detection element that would have the following advantages:

- Thinner than typical bulk material → low bias voltage (not kilovolts)
- Fewer structural defects → higher charge carrier lifetime → higher detection efficiency
- Lower porosity level → more nuclear reactions in given volume → higher detection efficiency

An alternative to a BN film detection element is very thin, robust, highly oriented bulk BN (including single crystal BN, when BN crystal growth is at an advanced enough stage).

In any case, successful implementation of a FIND device will require the continued refinement and use of methods for measuring the carrier mobility  $\mu$  and lifetime  $\tau$  (or the lifetime-mobility product  $\mu\tau$ ) of the BN detecting element. Measurement of the specific resistivity and chemical/ structural properties of the device electrical contacts is also crucial. Characterization of these BN and contact properties will be essential for screening and improving FIND devices, and ultimately for quality control.



# CONTENTS

<b>ACKNOWLEDGMENTS</b> .....	<b>i</b>
<b>EXECUTIVE SUMMARY</b> .....	<b>iii</b>
<b>INTRODUCTION AND BACKGROUND</b> .....	<b>1</b>
PROBLEM ADDRESSED AND INVESTIGATED SOLUTION .....	1
SOLID BORON NITRIDE FOR NEUTRON DETECTION .....	1
ADVANTAGES OVER EXISTING DETECTORS.....	1
PRACTICAL CONSIDERATIONS.....	2
Charge Carrier Recombination .....	2
Neutron Capture Efficiency .....	2
Electrode Contact Resistance .....	2
BN Conductivity.....	3
BULK BORON NITRIDE AS A DETECTOR ELEMENT .....	3
BORON NITRIDE FILM AS A DETECTOR ELEMENT.....	3
PROJECT PERSONNEL .....	4
<b>FIND DESCRIPTION AND MODELING</b> .....	<b>5</b>
GENERAL DESCRIPTION .....	5
CARRIER LIFETIME AND MOBILITY CALCULATIONS .....	6
EXPECTED DETECTOR PERFORMANCE .....	7
SUBSTRATE SELECTION FOR FILM GROWTH .....	9
<b>APPROACH AND METHODS</b> .....	<b>13</b>
BORON NITRIDE FILM GROWTH AND STRUCTURAL CHARACTERIZATION .....	13
CARRIER LIFETIME MEASUREMENTS.....	14
Microwave Cavity Perturbation.....	14
Time-Resolved Reflectivity.....	16
CARRIER MOBILITY MEASUREMENTS .....	18
ELECTRODE DEPOSITION AND PATTERNING .....	19
Electrode Deposition .....	19
Electrode Patterning.....	21
ELECTRICAL PROPERTIES CHARACTERIZATION .....	21
Electrodes .....	21
BN Films.....	22
THERMAL NEUTRON DETECTION METHODS.....	23
<b>RESULTS</b> .....	<b>25</b>
BORON NITRIDE FILM GROWTH AND STRUCTURAL CHARACTERIZATION .....	25
CARRIER LIFETIME MEASUREMENTS.....	30
Microwave Cavity Perturbation.....	30

Time-Resolved Reflectivity.....	32
CARRIER MOBILITY MEASUREMENTS.....	32
ELECTRODE ETCH RATES .....	33
ELECTRICAL PROPERTIES.....	34
Electrodes .....	34
BN Films.....	35
THERMAL NEUTRON DETECTION RESULTS .....	36
<b>SUMMARY AND CONCLUSIONS .....</b>	<b>39</b>
<b>RECOMMENDATIONS FOR FURTHER DEVELOPMENT.....</b>	<b>41</b>
<b>REFERENCES .....</b>	<b>43</b>
<b>APPENDIX A: CHARGE PULSE AMPLIFIER CIRCUIT.....</b>	<b>A-1</b>

## Figures

1. Two common crystal phases of boron nitride.....	4
2. Steady-current FIND detection circuit. ....	5
3. Block diagram of charge pulse amplifier circuit.....	5
4. Minimum acceptable mobility-lifetime product versus BN film resistivity .....	6
5. Two common growth planes of hexagonal boron nitride.....	10
6. Comparison of the sapphire and hBN (0001), or C-plane, surfaces. ....	11
7. Comparison of the MgO (100) and hBN (0001), or C-plane, surfaces.....	11
8. Schematic drawing of UHV BN film growth chamber at UMich.....	13
9. UHV BN film growth chamber and system at UMich.....	14
10. Microwave cavity perturbation technique. ....	15
11. Microwave cavity perturbation apparatus at VCU. ....	15
12. Carrier lifetime determination from MCP data.....	16
13. Schematic drawing of ultrafast time-resolved reflectivity system at UMich.....	17
14. Ultrafast time-resolved reflectivity measurement system at UMich.....	18
15. Corona discharge surface voltage measurement method .....	19
16. Schematic drawing of UHV ion beam sputtering system.. ....	20
17. UHV ion beam sputtering system.....	20
18. Deposition sequence of multilayer metal electrode.....	21
19. Silver wires connected to Ag/W/Ti electrodes on BN film sample OUT80. ....	22
20. BN film sample OUT77 mounted for <i>in-situ</i> furnace measurements.....	22
21. Charge pulse amplifier with neutron detector module.....	23
22. RHEED images before and after BN film SN021007 growth on (100) Si.....	25
23. FTIR spectrum of BN film SN021007 deposited on (100) Si.....	26

24. XRD spectrum of BN film SN021118 deposited on (100) Si.....	27
25. SEM photographs of BN film SN021118 deposited on (100) Si.....	28
26. Hexagonal BN film sample OUT81 on (100) MgO.....	28
27. FTIR spectrum of BN film SN030125 on (100) MgO.....	29
28. FTIR spectrum of BN film SN030813 on (100) high-resistivity Si. ....	30
29. Response of hBN film SN030125 on MgO using the MCP technique. ....	31
30. Sample current versus bias voltage for hBN bulk sample BLK12.....	32
31. Furnace cycle for Ag/W/Ti contacts on cBN-Si sample OUT71.....	34
32. Resistance between contacts versus temperature for cBN-Si sample OUT71.....	34
33. I-V characteristic between circular contacts on hBN/MgO sample OUT86.....	35
34. Bulk hBN sample BLK13 in FIND configuration.....	36
35. Charge pulse count rate for bulk hBN sample BLK13.....	37
36. Hexagonal BN film sample OUT86 on MgO with interdigitized electrodes. ....	37

## Tables

1. Variable symbols.....	7
2. Parameter symbols and values.....	7
3. BN film SN021007 deposition parameters.....	25
4. BN film SN021118 deposition parameters.....	26
5. XRD peak comparison.....	27
6. Reduced gas glow sample deposition parameters.....	29
7. Electrode metal wet etchants.....	33



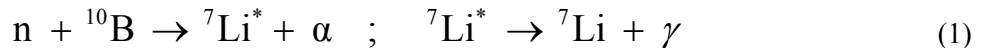
# INTRODUCTION AND BACKGROUND

## PROBLEM ADDRESSED AND INVESTIGATED SOLUTION

This research addresses the problem of efficient and convenient inspection of buildings, vehicles, persons, and other places for concealed nuclear materials (such as uranium or plutonium) that are being used, or capable of being used, in nuclear weapons. One way to determine the presence of nuclear materials is to detect the neutrons that are emitted from the atomic nucleus of these materials in the radioactive decay process. To overcome the problems encountered with conventional detectors, a solid-state analog of the gas proportional counter based on films or thin bulk pieces of boron nitride (BN) has been investigated. This new type of detector<sup>1</sup> is known as a Film Implementation of a Neutron Detector (FIND). For purposes of this report, both films and thin bulk pieces will be referred to as “films.”

## SOLID BORON NITRIDE FOR NEUTRON DETECTION

Neutrons can be detected by measurement of the secondary charged particles that result from nuclear reactions such as



The 2.3 MeV alpha particles from this reaction create electron-hole pairs in the material. Detection of these charge carriers before they recombine indicates the presence of the incident neutrons. The isotope boron-10, with its relatively large cross section for thermal neutrons (3837 barns), is particularly well suited for neutron detection, and is commonly used in gas-type counter detectors in the form of boron trifluoride gas,  $\text{BF}_3$ . Due to its greater density, a boron-containing solid detector would have a greatly enhanced total cross section for neutrons, and thus far better detector sensitivity. For example, the total cross section increases by a factor of about 3000 in going from  $\text{BF}_3$  gas (at room temperature and atmospheric pressure) to solid boron nitride, BN. In addition, the wide bandgap of BN (around 5 to 6 eV) means better room temperature operation than semiconductor solid-state nuclear particle detectors because of reduced thermally induced recombination of electrons and holes. Finally, pure BN is a very stable compound that can withstand large variations in temperature and humidity without degradation, and thus is suitable for use in a portable detector unit that could be deployed in varied environments.

## ADVANTAGES OVER EXISTING DETECTORS

Compared to commonly used neutron detectors, such as gas proportional counters and scintillation counters, the FIND device is much more compact, and therefore portable. The detecting element consists of a substrate that supports a boron nitride film sandwiched by electrode layers. The total thickness of the detector element is typically less than 1 mm. The area of a single detector element is  $1 \text{ cm}^2$  or smaller (depending on the BN thickness and resistivity). Large area detectors would consist of an array, or mosaic, of single detector elements. Because the voltage applied across the BN film is on the order of a few volts, compared to kilovolts for standard detectors, problems associated with high voltage (arcing, and the extra space or insulation needed to prevent arcing) are avoided. Operation at low voltage also means that the electronics used to apply the electrode voltage and to measure the detector current can be simpler, more compact, safer to the user, and much less power consuming. Additionally, the FIND device does not use exotic high-purity gases (or the special means to contain the gases at high pressure) required by gas proportional counter detectors. Solid-state neutron detectors based on silicon or germanium photodiodes and phototransistors have been designed also,

but they are much smaller in area than the FIND device, and therefore less sensitive. They also typically require a neutron converter foil, such as gadolinium, in front of the semiconductor device.

## PRACTICAL CONSIDERATIONS

There are a number of issues to consider in using solid BN for neutron detection, including:

- Charge carrier recombination
- Neutron capture efficiency
- Electrode contact resistance
- Conductivity of the BN

### Charge Carrier Recombination

The BN must be sufficiently defect-free for this type of detector to work. Otherwise, the free carriers produced by the nuclear reaction will be captured at defect sites before they can reach the detector electrodes. Electron-hole recombination (by this or other mechanisms) will be minimized if the carrier transit time through the material thickness,  $\tau_t$ , is much less than the recombination time, or carrier lifetime,  $\tau$ . The transit time, determined by the BN thickness, the carrier mobility  $\mu$ , and the applied electric field  $E$ , is equal to

$$\tau_t = \frac{d}{\mu E} = \frac{d^2}{\mu V} . \quad (2)$$

where  $d$  is the BN thickness, and  $V$  is the voltage across this thickness. The carrier lifetime and mobility are not well known for BN, and both likely depend on crystal phase (hexagonal or cubic), purity, carrier concentration, etc. Of fundamental interest is the mobility-lifetime product  $\mu\tau$ , which is the average distance traveled by a free carrier, per unit electric field, before recombination occurs. Recombination will not be a problem if  $\tau \geq \tau_t$ , or equivalently, if

$$\mu\tau \geq d^2/V , \quad (3)$$

For a practical working device,  $\mu\tau$  should be several times the minimum value given by Equation 3.

### Neutron Capture Efficiency

The BN thickness also directly influences the neutron capture efficiency. For example, to absorb close to 100% of normally incident neutrons, a cubic-phase BN (cBN) detecting element would have to be about 150  $\mu\text{m}$  thick (based on a BN density of 3.5  $\text{g}/\text{cm}^3$ , and the thermal neutron reaction cross section and 19.6% natural abundance of  $^{10}\text{B}$ ). Depending on the values of  $\mu$  and  $\tau$  in BN, there will be a thickness trade-off between carrier recombination time and neutron capture efficiency.

### Electrode Contact Resistance

The electrical contact between the BN detecting element and the electrodes must be conducting enough that the free carrier current generated by the nuclear reaction is not blocked from flowing in the external measurement circuit. If the resistance of the contacts is small compared to that of the BN film, then essentially all of the electric field produced will be across the BN, as needed to sweep out any free charge. One of the largest hurdles to a solid-state BN neutron detector is the ability to make low-resistance contacts to the material. Such low-resistance contacts are needed so that the potential applied between the top and bottom electrodes on the detecting element gives a voltage drop mainly

across the BN and not across the BN/electrode interfaces. An ohmic contact (linear current-voltage characteristic) would ensure that this condition is met, and is preferable to a Schottky-barrier contact (non-linear current-voltage characteristic and typically higher contact resistance). The FIND device would work with either type of contact, however, as long as the contact resistance is small compared to that of the BN film.

### **BN Conductivity**

Another important consideration is the electrical conductivity of BN. The material must be conducting enough to permit the signal current (due to free carriers generated by the nuclear reaction) to flow to the detector electrodes. But it must also be insulating enough that (1) the voltage difference between the detector electrodes required to attract the free carriers to the electrodes is of the order of a few volts, and (2) the dark current is low enough that it does not interfere with measurement of the signal current. The BN conductivity presumably can be adjusted if necessary by controlled impurity doping during manufacture.

### **BULK BORON NITRIDE AS A DETECTOR ELEMENT**

A thin plate of bulk boron nitride may be used as the neutron-sensitive material in the FIND device. Only polycrystalline, hexagonal-phase BN (hBN), typically formed from pressed powder, is made commercially in sizes large enough for this application. The purest material readily available (> 99.29% pure) is Combat<sup>®</sup> AX05 grade manufactured by the Saint-Gobain Advanced Ceramics Corporation (formerly The Carborundum Company). Using this bulk material has serious drawbacks, however, compared to high-quality vapor-deposited films, including:

- Small grain size and high porosity level → high density of carrier traps → low carrier lifetime
- High porosity level → fewer reactions in given volume → decreased detection efficiency
- Low mechanical strength → must be thicker than films → high bias voltage required

But because bulk hBN can be purchased with a reasonably high purity and high resistivity (>  $10^{14}$  Ω-cm), it is useful as a FIND detector element, at least for testing and demonstration of the concept. Combat<sup>®</sup> AX05 grade hBN was therefore used for the bulk samples of this report.

### **BORON NITRIDE FILM AS A DETECTOR ELEMENT**

To use solid boron nitride as a neutron detector, one must be able to collect the free electrons that are created by the above reaction. An electric field applied across the BN can be used to sweep up these charge carriers. Because of the relatively small distances involved (the film thickness), applied voltages on the order of a few volts will suffice (rather than the kilovolts needed for bulk samples). However, the electrons must reach the electrodes that produce the field before they recombine with the simultaneously generated holes or with charge-trapping crystal defects. Solid BN, usually sintered from powder, contains many defects, including boron or nitrogen vacancies, impurities, grain boundaries, and porosity. Materials grown as films, deposited under the right conditions, can have better crystalline perfection and purity, and therefore fewer defects, than bulk polycrystalline solids. In the case of BN, growth as a film allows the choice of two different crystal phases, a hexagonal structure (hBN) analogous to graphite, and a cubic form (cBN) analogous to diamond (see Figure 1). Large bulk pieces of boron nitride are available only in the hexagonal phase. The two phases have different densities, electrical resistivities, and carrier mobilities. Based on these properties, one BN phase may be better suited for neutron detection than the other.

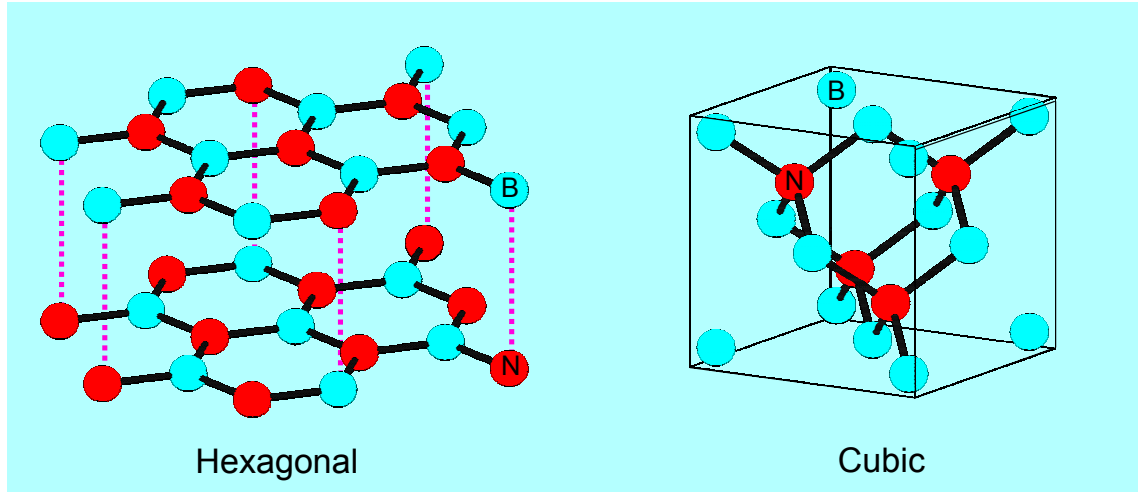


Figure 1. Two common crystal phases of boron nitride.

## PROJECT PERSONNEL

The boron nitride thin films studied in this research were provided and structurally characterized by the University of Michigan (UMich, under SSC San Diego contract number N66001-97-D-5028, delivery order 83). The UMich personnel involved in this effort include Dr. Roy Clarke (professor and director of the Applied Physics Program), Pedro Encarnación (graduate research assistant), and Abishai Daniel (graduate research assistant).

The carrier lifetime in thin films and bulk pieces of hexagonal boron nitride has been investigated by Virginia Commonwealth University (VCU, under SSC San Diego contract number N66001-97-D-5028, delivery order 84) using a Microwave Cavity Perturbation (MCP) technique. The VCU personnel involved in this effort include Dr. Gary Tepper (associate professor in the Department of Mechanical Engineering) and Dr. Royal Kessick (post-doctoral student).

The remainder of the project tasks were performed at SSC San Diego. The primary SSC San Diego personnel working on this project are Dr. Wayne McGinnis (the author), Jennifer Beyer (graduate student contractor; masters degree candidate in the Department of Chemistry at San Diego State University), and Dr. Manjit Randhawa (visiting professor from Southern University, Baton Rouge). Other SSC San Diego personnel contributing to the project include Dr. Jon Losee, Ron Brockus, and Ed Wesley.

## FIND DESCRIPTION AND MODELING

### GENERAL DESCRIPTION

A schematic representation of the FIND detector circuit is shown in Figure 2. Current is measured with the ammeter, and the resistor value controls the voltage drop across the BN film. This circuit is most useful for neutron flux levels high enough to generate a steady current that flows in addition to the background, or dark, current. The total measured current is the sum of the dark current and this additional, or excess, current.

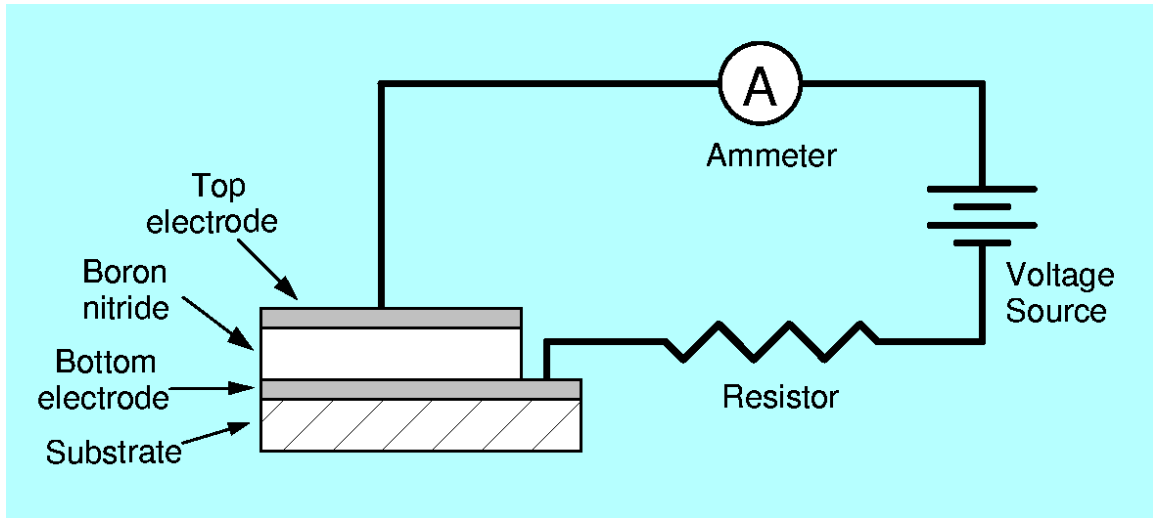


Figure 2. Steady-current FIND detection circuit.

For low neutron flux levels, the excess current is in the form of current pulses. In this case, a charge pulse amplifier circuit can be used to detect these pulses. The amplified pulses can then be counted with a standard pulse counting instrument. For both measurement methods, the excess current is due to the free charge carriers produced by the interaction of thermal neutrons with the BN film in the detector element. The amplitude of a continuous excess current, or the signal rate of charge pulses, is therefore proportional to the neutron flux at the detector. A block diagram of the charge pulse amplifier circuit is shown in Figure 3. The details of this circuit are in Appendix A: CHARGE PULSE AMPLIFIER CIRCUIT. The charge sensitive preamplifier is an Amptek A250.

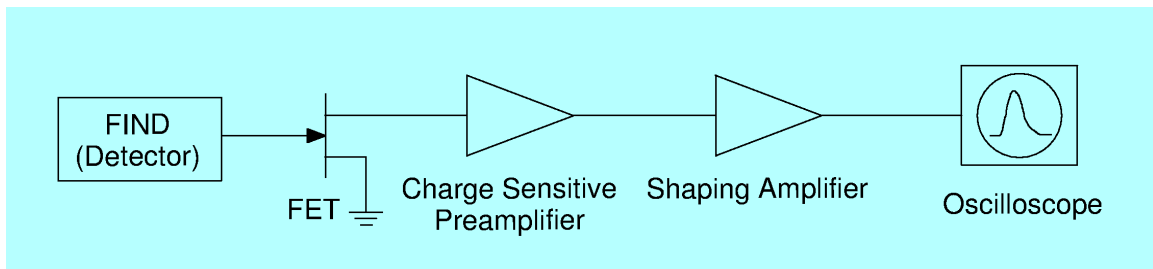


Figure 3. Block diagram of charge pulse amplifier circuit.

## CARRIER LIFETIME AND MOBILITY CALCULATIONS

As discussed under PRACTICAL CONSIDERATIONS, the BN film properties must be such that electrical carriers generated after the nuclear reaction of Equation 1 are able to reach the device electrodes (see Figure 2). The minimum value of the mobility-lifetime product  $\mu\tau$  for which the FIND device will work is that for which the carrier lifetime  $\tau$  is equal to the carrier transit time  $\tau_t$  across the BN film thickness. The voltage  $V$  across the BN film is given by

$$V = \frac{I\rho d}{A}, \quad (4)$$

where  $I$  is the current flowing across the film thickness and  $\rho$  is the electrical resistivity of the film. Combining Equations 2 and 4, the carrier transit time  $\tau_t$  is given by

$$\tau_t = \frac{dA}{\mu I\rho}. \quad (5)$$

This minimum value of  $\mu\tau$ , calculated from Equation 2, is shown in Figure 4 for a BN film  $1\mu\text{m}$  thick and  $1\text{ cm}^2$  in area, and a dark current of  $1\text{ nA}$ .

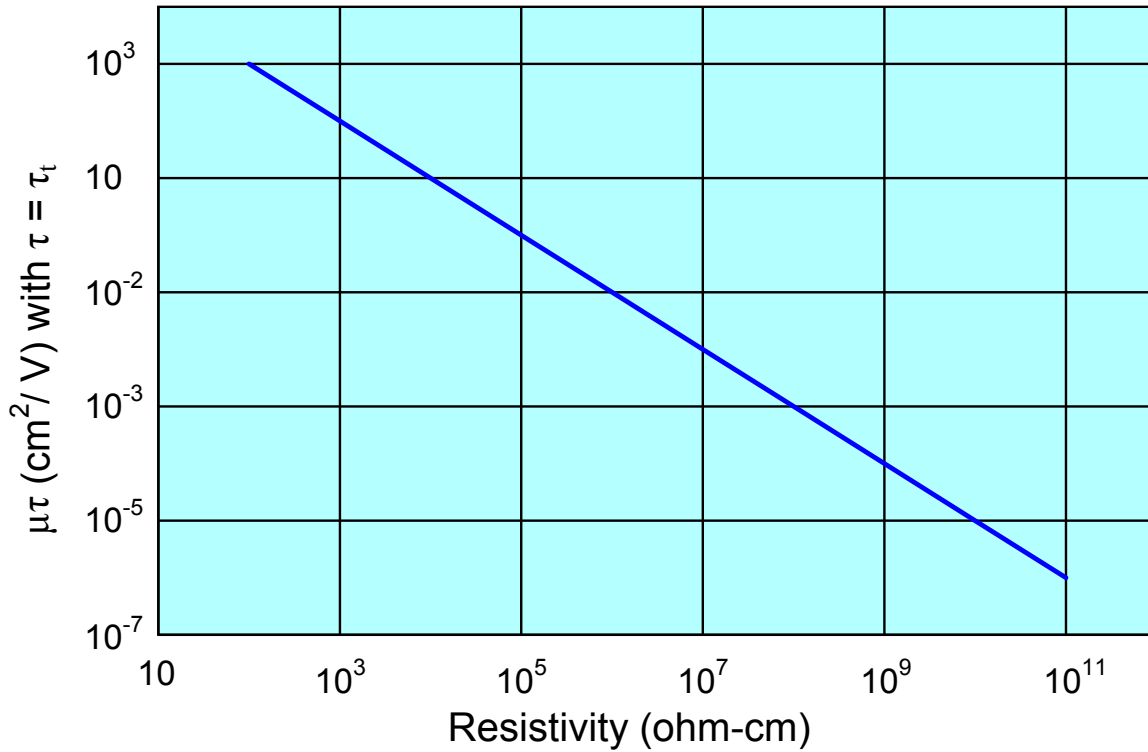


Figure 4. Minimum acceptable mobility-lifetime product versus BN film resistivity (with a dark current of  $1\text{ nA}$ , film thickness  $d = 1\mu\text{m}$ , and film area  $A = 1\text{ cm}^2$ ).

## EXPECTED DETECTOR PERFORMANCE

Expressions for the expected amplitude  $V_p$  of the output pulses from the Amptek A250 charge sensitive preamplifier (see Figure 3), the measured nuclear reaction rate  $v$ , and the sensitivity  $S$  are given below in terms of the variables and parameters listed in Tables 1 and 2.

Table 1. Variable symbols.

Symbol	Quantity
$\mu$	carrier mobility
$\tau$	carrier lifetime
$E$	applied electric field
$V$	applied voltage
$d$	BN thickness
$A$	electrode area
$V$	BN volume between electrodes
$\zeta$	charge collection efficiency
$S$	sensitivity
$\Phi$	neutron flux density
$\Sigma$	detector total cross section for thermal neutrons
$r$	distance to neutron point source

Table 2. Parameter symbols and values.

Symbol	Quantity	Value
$\rho_{BN}$	BN mass density	2.28 g/cm <sup>3</sup>
$M_B$	boron molecular weight	10.811 g/mole
$M_N$	nitrogen molecular weight	14.0067 g/mole
$M_{BN}$	BN molecular weight	24.8177 g/mole
$N_A$	Avagadro's number	$6.02 \times 10^{23}$ /mole
$n_B$	boron atom number density	$5.53 \times 10^{22}$ /cm <sup>3</sup>
$\sigma_{B-10}$	<sup>10</sup> B cross section for thermal neutrons	$3837 \times 10^{-24}$ cm <sup>2</sup>
$\sigma_B$	effective thermal neutron cross section of B in natural BN	$764 \times 10^{-24}$ cm <sup>2</sup>
$\epsilon_\alpha$	$\alpha$ -particle energy for reaction of Equation 1	1.47 MeV
$\epsilon_{e-h}$	electron-hole creation energy for BN	~ 14.5 eV
$S_{amp}$	sensitivity of Amptek A250 charge pulse preamplifier	0.16 $\mu$ V/electron
$\Lambda$	total neutron generation rate of AmBe source	$10^5$ / s

The number  $N$  of free carriers generated in each reaction (Equation 1) is  $2\varepsilon_\alpha/\varepsilon_{e-h} \approx 2 \times 10^5$ . The expected amplitude  $V_p$  of an output pulse from the Amptek A250 charge sensitive preamplifier is then

$$V_p = \begin{cases} N \cdot S_{\text{amp}} \approx 32 \text{ mV} & (\text{e and h}) \\ \frac{N}{2} \cdot S_{\text{amp}} \approx 16 \text{ mV} & (\text{e or h}) \end{cases} \quad (6)$$

The upper value in Equation 6 corresponds to the case where both the free electrons and holes reach the device electrodes, while the lower value corresponds to the case where only electrons or only holes reach one of the device electrodes. In general,  $V_p$  will depend on the relative values of the electron and hole mobilities and lifetimes in BN. For a given reaction,  $V_p$  will depend on the thickness of the BN and the exact location of the reaction within the BN.

For a detector not limited by the carrier mobility-lifetime product (i.e., Equation 3 is easily satisfied), the expected nuclear reaction rate  $v_o$ , in terms of the detector's total cross section for thermal neutrons  $\Sigma$  and the neutron flux density  $\Phi$ , is given by

$$v_o = \Sigma \Phi \quad (7)$$

The measured nuclear reaction rate  $v$  is given by

$$\begin{aligned} v &= \zeta v_o \\ &= \zeta \Sigma \Phi \\ v &= S \Phi \end{aligned} \quad (8)$$

where  $\zeta$  is the charge collection efficiency (a mobility-lifetime limitation factor;  $0 \leq \zeta \leq 1$ ) and  $S = \zeta \Sigma = v/\Phi$  is the sensitivity (an effective cross section for thermal neutrons). Other factors that might reduce  $v$  compared to  $v_o$ , such as absorption by air, are ignored here because, in this case, they should have little effect compared to  $\zeta$ . For a point neutron source at a distance  $r$  from the detector,  $\Phi = \Lambda/(4\pi r^2)$ , and the reaction rate is

$$v = \frac{S \Lambda}{4\pi r^2} \quad (9)$$

where  $\Lambda$ , the total neutron generation rate of the source, is given in Table 2 for the  $^{241}\text{Am}$ -Be sealed source used in this research.

The detector sensitivity  $S$  can also be expressed in terms of the BN material properties  $n_B$ ,  $\sigma_B$ ,  $\mu$ , and  $\tau$ , and the detector parameters  $A$ ,  $V$ , and  $d$ . First, the mean free path  $x$  of a free charge carrier in BN is given by

$$\begin{aligned} x &= v \tau \\ &= \mu E \tau \\ x &= \frac{\mu \tau V}{d} \end{aligned} \quad (10)$$

where  $v$  is the carrier drift velocity reached in the applied electric field  $E$  (due to the application of voltage difference  $V$  across BN thickness  $d$ ).<sup>†</sup> The total charge collection distance is  $2x$ .

The charge collection efficiency  $\zeta$  can be written, for  $d \geq 2x$ , as

$$\zeta = \frac{2x}{d} = \frac{2\mu\tau V}{d^2} . \quad (11)$$

The total cross section for thermal neutrons  $\Sigma$  is given by

$$\Sigma = n_B \sigma_B V = n_B \sigma_B A d \quad (12)$$

where  $n_B = \rho_{BN} N_A / M_{BN}$  and  $M_{BN} = M_B + M_N$ . From Equations 8, 11, and 12, the sensitivity  $S$  is then <sup>‡</sup>

$$S = (2 n_B \sigma_B \mu \tau) \cdot \left( \frac{AV}{d} \right) . \quad (13)$$

Note that the first quantity in parentheses in Equation 13 contains only material property parameters, while the second quantity contains only experimental parameters (detector geometry and applied voltage).

## SUBSTRATE SELECTION FOR FILM GROWTH

A crystal visualization software package, LATUSE,<sup>2</sup> has been used to determine which single-crystal substrates are best suited for the growth of the hBN films. This determination was directed toward the hexagonal phase, rather than the cubic phase, because of the relative ease of growing high-resistivity hBN films compared to cBN films. This computer program enabled the comparison of hBN lattice spacings (see Figure 5 for two common BN growth surfaces) with those of commonly available insulating substrates (e.g., sapphire, magnesium oxide, quartz, etc.), and thus the selection of substrates favorable to epitaxial growth, if possible, of BN films. Note that the three columns of atoms in the A-plane correspond to three C-plane layers that have been rotated 90°, left to right. The right-hand column of atoms in the C-plane therefore matches the left-hand column of atoms in the A-plane. Only atoms and bonds on the crystal surface are shown in this and subsequent figures.

---

<sup>†</sup> Here, and in subsequent equations,  $\mu\tau$  is understood to represent an average of the mobility-lifetime products for free electrons and holes. That is,  $\mu\tau = (\mu_e \tau_e + \mu_h \tau_h) / 2$ . If  $\tau_e = \tau_h$ , then  $\mu = (\mu_e + \mu_h) / 2$  represents the average mobility of electrons and holes.

<sup>‡</sup> Note that if  $\mu_e \tau_e \gg \mu_h \tau_h$ , for example, then  $S = (n_B \sigma_B \mu_e \tau_e) \cdot (AV/d)$  and  $\zeta = \mu_e \tau_e V / d^2$ .

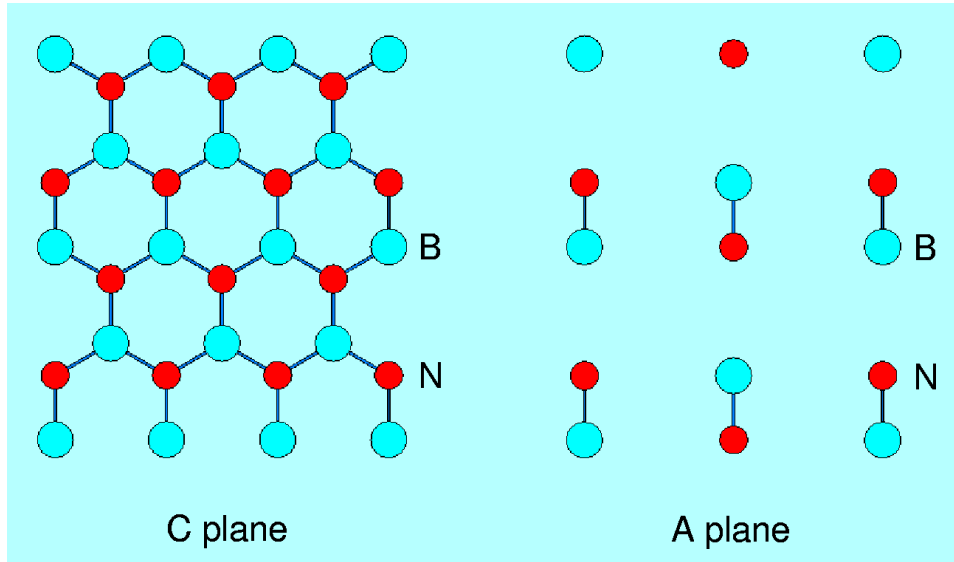


Figure 5. Two common growth planes of hexagonal boron nitride.

Example comparisons between the hBN C-plane surface and two common substrate materials, sapphire ( $\text{Al}_2\text{O}_3$ ) and magnesium oxide ( $\text{MgO}$ ), are shown in Figure 6 and Figure 7, respectively. As seen in these figures, MgO seems to be a somewhat better match to this hBN surface structure than sapphire.

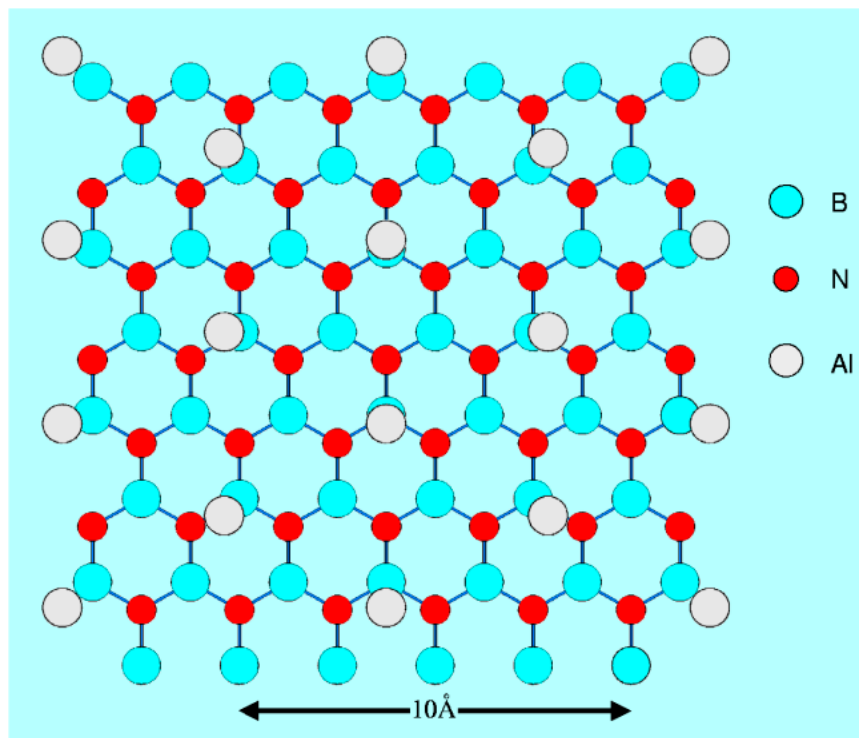


Figure 6. Comparison of the sapphire and hBN (0001), or C-plane, surfaces.

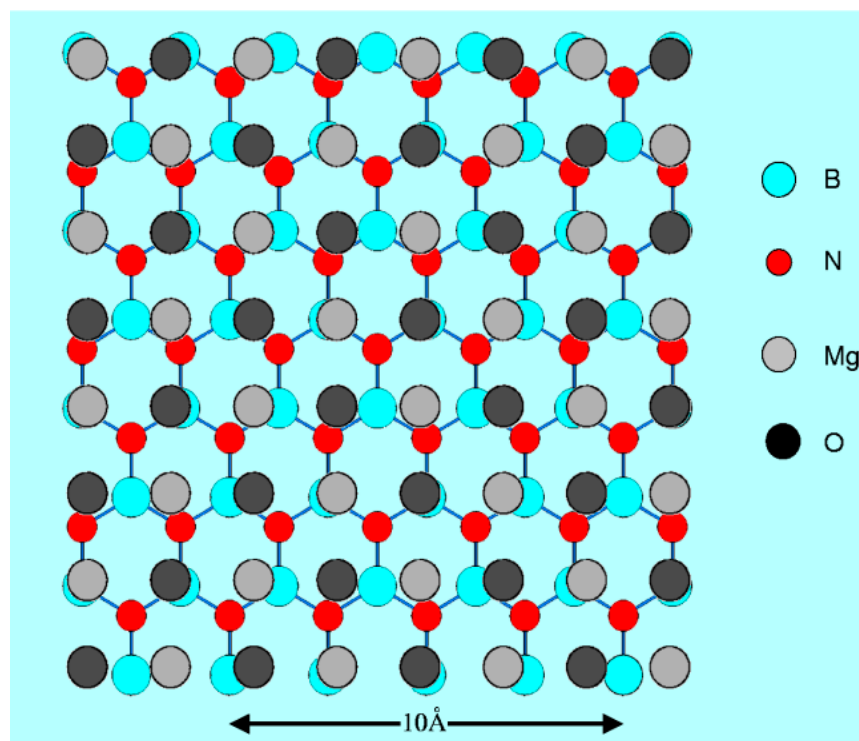


Figure 7. Comparison of the MgO (100) and hBN (0001), or C-plane, surfaces.



## APPROACH AND METHODS

### BORON NITRIDE FILM GROWTH AND STRUCTURAL CHARACTERIZATION

The BN films were deposited at UMich by magnetron sputtering of a hexagonal boron nitride target in an ultrahigh vacuum (UHV) chamber. Energetic nitrogen ions generated by a Tectra Electron Cyclotron Resonance (ECR) source were directed at the growing films. The ion energy was controlled by a D.C. bias applied to the substrate. This bias voltage is crucial in determining if the BN films are grown in the hexagonal phase or in the cubic phase. A reduced bias growth process is used in some cases.<sup>3</sup> The substrates used for this research were either single crystal (100) silicon or (100) magnesium oxide. The substrate temperature during film growth of 1000°C is believed to facilitate the heteroepitaxial formation of the boron nitride film on the substrate surface. The growth chamber is shown in Figures 8 and 9.

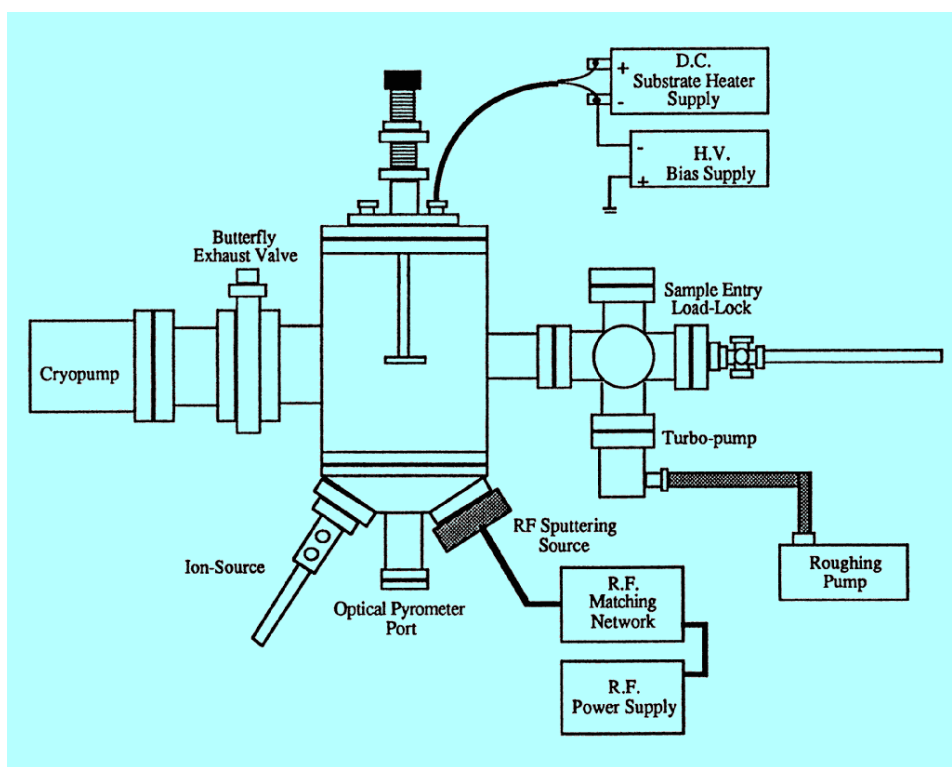


Figure 8. Schematic drawing of UHV BN film growth chamber at UMich.

The crystal structure of the BN films was studied by *in-situ* Reflection High-Energy Electron Diffraction (RHEED) and by X-Ray Diffraction (XRD, using a 16 keV synchrotron radiation beam line of the Advanced Photon Source at Argonne National Laboratory). The crystal phase composition of the films was characterized with Fourier Transform Infrared (FTIR) spectroscopy. Film morphology was examined by Scanning Electron Microscopy (SEM).



Figure 9. UHV BN film growth chamber and system at UMich.

## CARRIER LIFETIME MEASUREMENTS

### Microwave Cavity Perturbation

The carrier lifetime in thin films and bulk pieces of hexagonal boron nitride has been investigated at VCU using a Microwave Cavity Perturbation (MCP) technique. Figure 10 is a schematic diagram illustrating the basic experimental configuration of this technique. As shown in Figure 11, a tunable solid-state YIG oscillator provides the microwave energy with a frequency range of 4 to 8 GHz and a maximum power output of 100 mW. The microwave energy is directed through a waveguide and enters through an adjustable aperture into a  $TM_{010}$  cylindrical resonant cavity containing the sample. The resonant frequency of the cavity is determined by its size and by the dielectric constant of the sample material, and is approximately 5 GHz for the experiments reported here. The  $TM_{010}$  resonant mode provides a maximum electric field at the center of the cavity. The electric field magnitude can be estimated by balancing the cavity input power with the cavity loss under equilibrium conditions.

The change in the quality factor ( $Q$ ) of the microwave cavity upon photoexcitation of the sample is the basis for the technique. A 1-mm-diameter circular aperture was machined into the side of the cavity for the laser illumination. The sample is inserted axially into the center of the cavity using a cylindrical beryllium oxide (BeO) cold-finger. BeO is an electrical insulator and creates negligible load to the cavity in comparison to the BN sample. However, the thermal conductivity of BeO is quite high, and the sample temperature can be controlled by adjusting the temperature of the external end of the BeO rod without introducing coolant directly into the cavity. Condensation inside the cavity is avoided by keeping the cavity under a constant positive pressure of inert gas. The BeO rod allows the evaluation of lifetime measurements at room temperature and at liquid nitrogen temperature (77 K).

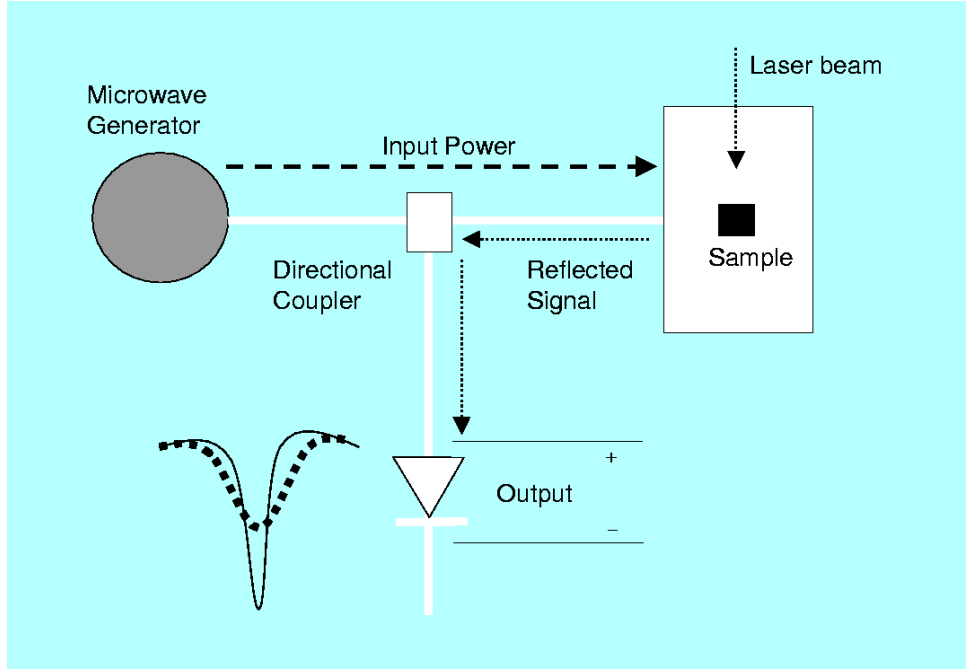


Figure 10. Microwave cavity perturbation technique.

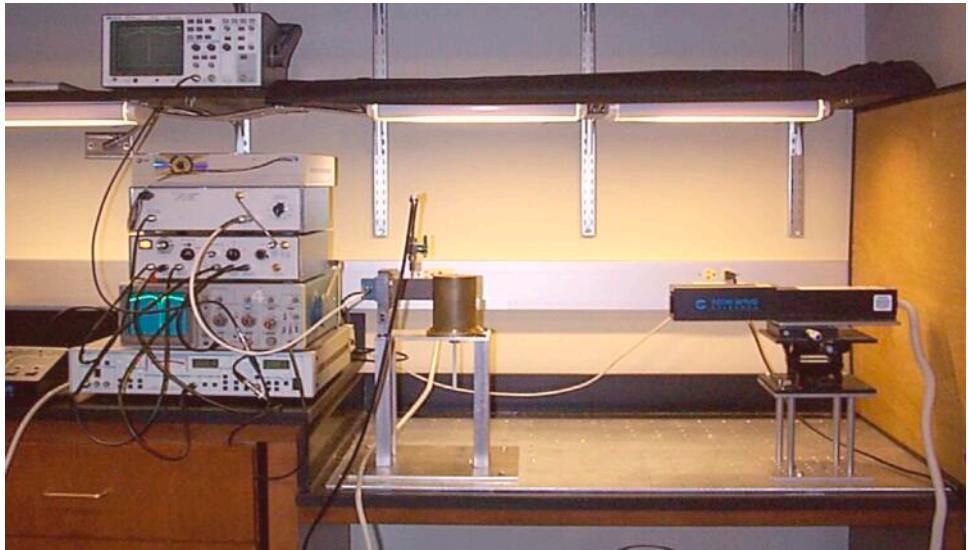


Figure 11. Microwave cavity perturbation apparatus at VCU.

After the photoexcitation is removed, the conductivity of the sample and quality factor of the cavity return to the equilibrium values at a rate dependent on the electronic decay process in the sample. The change in the cavity quality factor is detected through the corresponding change in the reflected microwave power. Thus, the decay time is determined by observing the time dependence of the reflected microwave power immediately following the sample excitation,<sup>4</sup> as shown in Figure 12. In the figure, the carrier density in the sample increases from  $n_0$  to  $(n_0 + \tau G)$  when irradiated with light of frequency  $\nu$ . When the light is turned off at  $t = 0$ , the carrier density decays back to its “dark” value with a characteristic decay time defined as the carrier lifetime,  $\tau$ . The generation rate of carriers during photoexcitation is given by the constant  $G$ . The carrier lifetime  $\tau$  can be determined from the

initial (linear) part of the decay curve, where  $n(t) \approx n_0 + \tau G[1 - (t/\tau)]$ , in which case  $n = n_0$  when  $t = \tau$ .

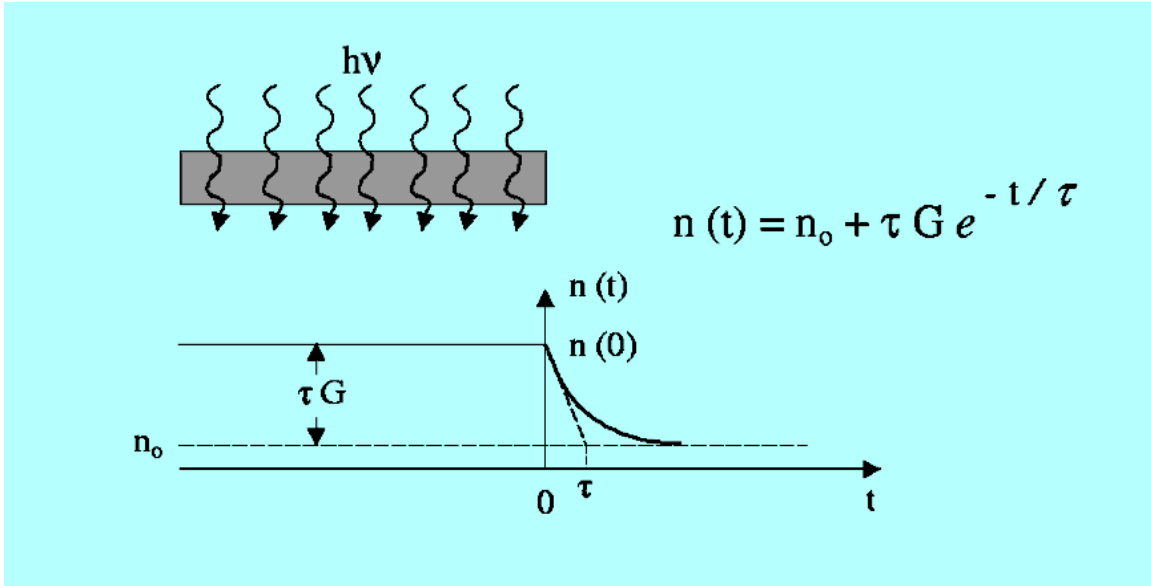


Figure 12. Carrier lifetime determination from MCP data.

### Time-Resolved Reflectivity

The time-resolved reflectivity (TRR) method, shown schematically in Figure 13, can be used to measure carrier lifetimes shorter than those that can be determined by the MCP technique. In the TRR method, the intensity of a laser beam reflected from the sample surface is measured as a function of time. This time-resolved intensity is proportional to the free charge carrier density at the sample surface, enabling determination of the carrier lifetime using the type of analysis shown in Figure 12. A pulsed Ti-sapphire laser, with a repetition rate of 82 MHz and a pulse width of 40 fs, provides a pulsed laser beam that is split into pump and probe beams in a 10:1 intensity ratio, respectively. Figure 14 shows the optics needed to bring the pump and probe laser beams into spatial and temporal coincidence at the surface of the sample. Both beams are focused onto the sample with respective spot diameters of 100 and 50  $\mu\text{m}$ . The pump beam is s-polarized, while the probe is p-polarized. The pump and the probe beams are modulated with a photoelastic modulator at 50 kHz, and a mechanical chopper at 60 Hz, respectively. The reflectivity signal is measured by a lock-in amplifier/photodiode combination. The probe beam is delayed with respect to the pump beam by means of a translation stage delay rail, with a delay range of 0 to 600 ps. The time-resolution of the measurement is approximately 200 fs.

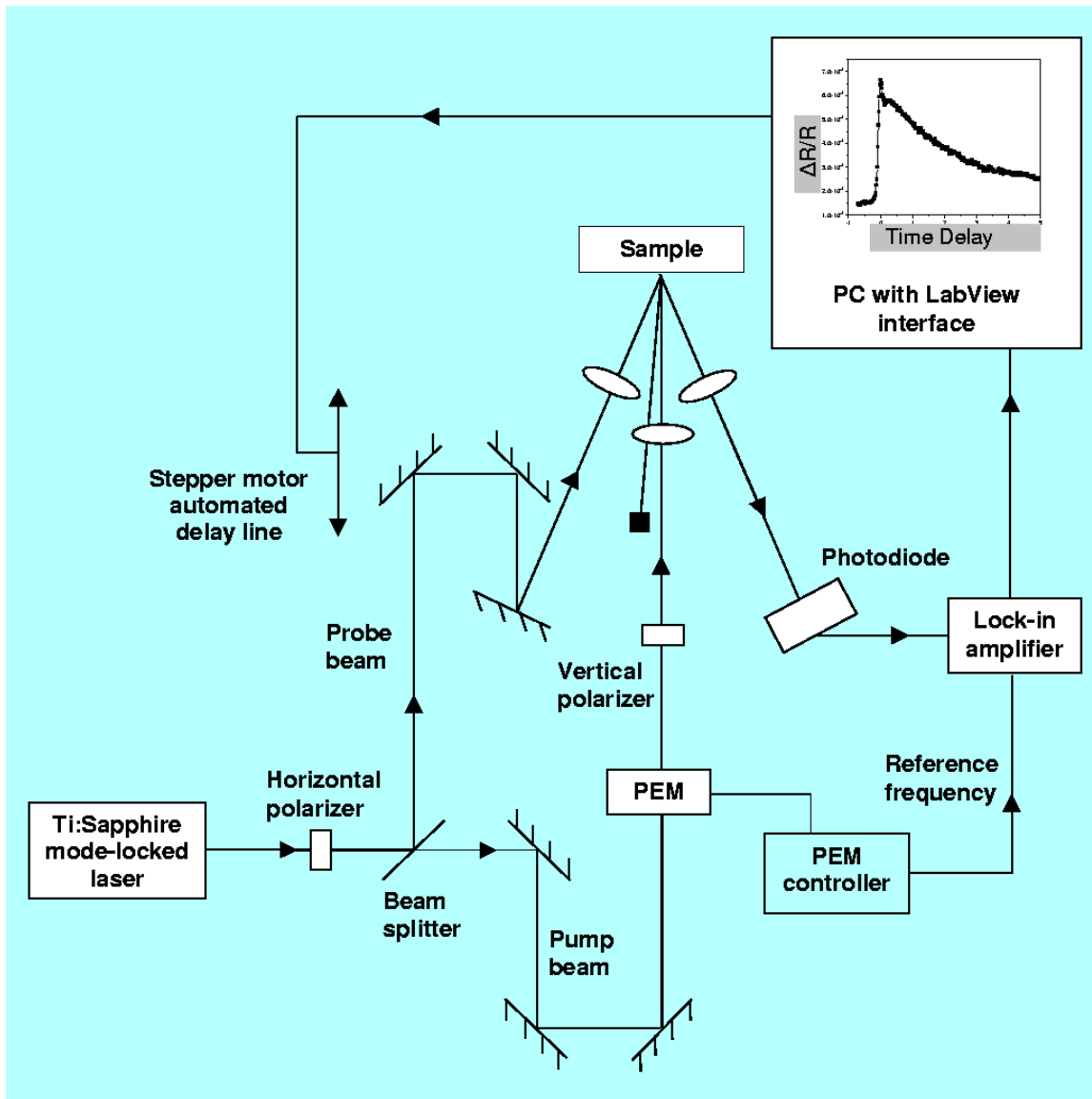


Figure 13. Schematic drawing of ultrafast time-resolved reflectivity system at UMich.

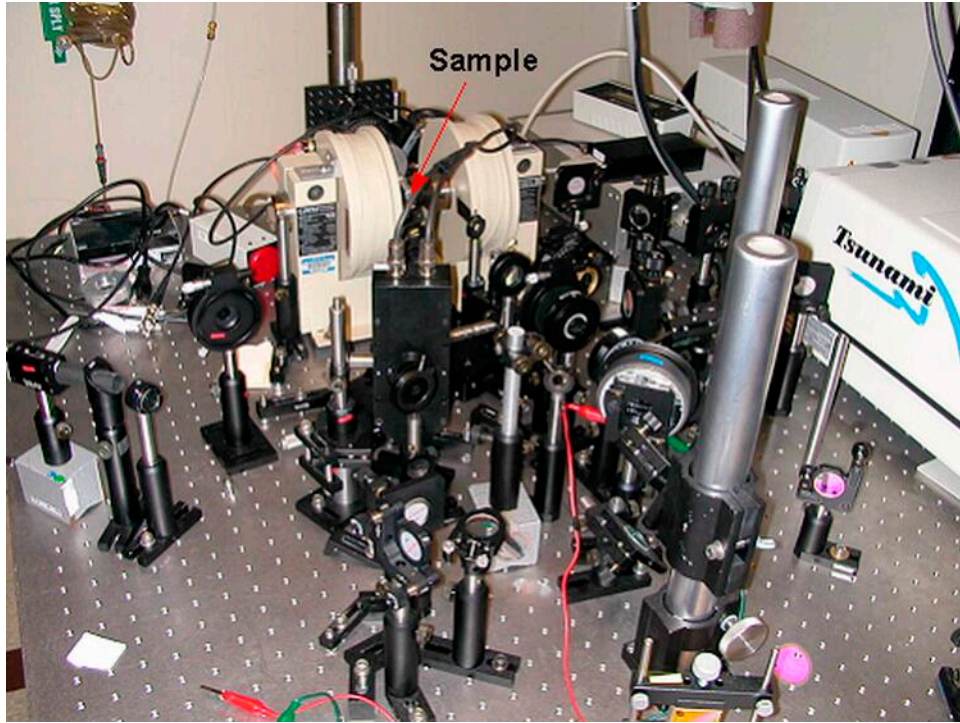


Figure 14. Ultrafast time-resolved reflectivity measurement system at UMich.

### CARRIER MOBILITY MEASUREMENTS

A corona discharge method of determining the carrier drift mobility of highly insulating BN from the time decay of a surface voltage was investigated. In this technique, the sample is prepared with a grounded metallic electrode on its bottom surface (see Figure 15). A high voltage (around 7 to 10 kV) is applied, relative to ground, to a needle-shaped electrode positioned a few centimeters above the free surface of the film (i.e., the non-electroded surface). The film's free surface is also surrounded by a grounded metal shield. The high voltage produces a so-called corona discharge (a plasma consisting of electrons and ionized air or water molecules) at the tip of the needle. The ions follow the electric field lines to the metal shield and to the film's free surface. The film surface charges up, thus producing a potential difference  $V$  between the surface and the grounded back side of the film. An electron (or hole) current  $I$  flows through the film thickness due to this potential difference and neutralizes the arriving ions. In the steady state, this current is equal to the current arriving at the surface from the corona discharge. If the discharge is turned off, the surface potential  $V_s$  will decay with time. Under space-charge-limited<sup>5</sup> constant current conditions, this decay has been shown to depend in a simple way on the sample thickness and the carrier drift mobility  $\mu$ .<sup>6,7</sup> The mobility can be determined from the time decay of the surface voltage. Under space-charge-limited (SCL) conditions, for a trap-free insulator, the current will be related to the voltage by<sup>8</sup>

$$I = \frac{9}{8} \epsilon \mu \frac{V^2 A}{L^3}, \quad (14)$$

where  $\epsilon$  is the boron nitride dielectric constant. In the absence of SCL conditions, the current will be related to the voltage by Ohm's law:

$$I = n e \mu \frac{VA}{L}, \quad (15)$$

where  $n$  is the carrier density and  $e$  is the electron charge. Ohmic current-voltage characteristics can be due to dominance of surface conduction (leakage current) around the sample surface over bulk conduction through the sample.<sup>9</sup>

So-called time-of-flight techniques, in which the transit time needed for an injected sheet of free charge carriers to traverse the sample thickness under constant voltage conditions is measured, have also been used to determine  $\mu$ .<sup>10</sup> In this case, the sheet of charge is generated (in a time short compared to the transit time) by various means, including pulsed irradiation by intense light (exciting carriers across the bandgap),<sup>10</sup>  $\alpha$ -particles,<sup>11</sup> and high-energy electrons.<sup>12,13</sup>

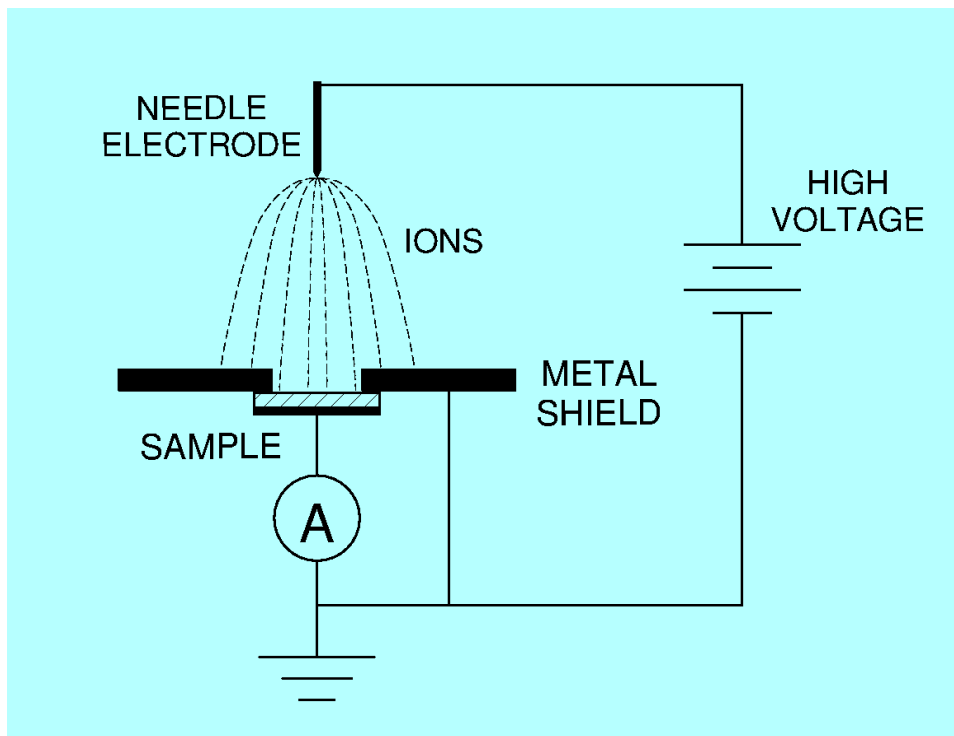


Figure 15. Corona discharge surface voltage measurement method.

## ELECTRODE DEPOSITION AND PATTERNING

### Electrode Deposition

The conducting electrodes for the FIND device (see Figure 2) consist of multilayer metal films deposited using the UHV ion beam sputtering system shown in Figures 16 and 17. The BN electrical contact method used here is similar to that developed at SSC San Diego to make contact to semiconducting diamond.<sup>14</sup> In that case, a metal such as Mo is deposited onto the diamond substrate or film and then furnace annealed, reacting with carbon to form conducting molybdenum carbide. The semiconducting-diamond/carbide combination forms an ohmic contact. For the case of boron nitride, titanium metal (followed by diffusion barrier and contacting layers) is used to coat semiconducting c-BN, and the sample is then heated in an inert-atmosphere. Ti reacts with BN to form titanium

nitride and titanium borides, both of which are conducting. A barrier layer of W prevents formation of titanium oxides (during atmospheric transfer of the samples) and their subsequent diffusion through a Au or Ag contacting layer (to which wire bonds may be formed). The deposition sequence of the multilayer electrode is shown in Figure 18. Titanium-based contacts have recently been evaluated by the author in a project to characterize the electronic properties of cBN films.<sup>15</sup>

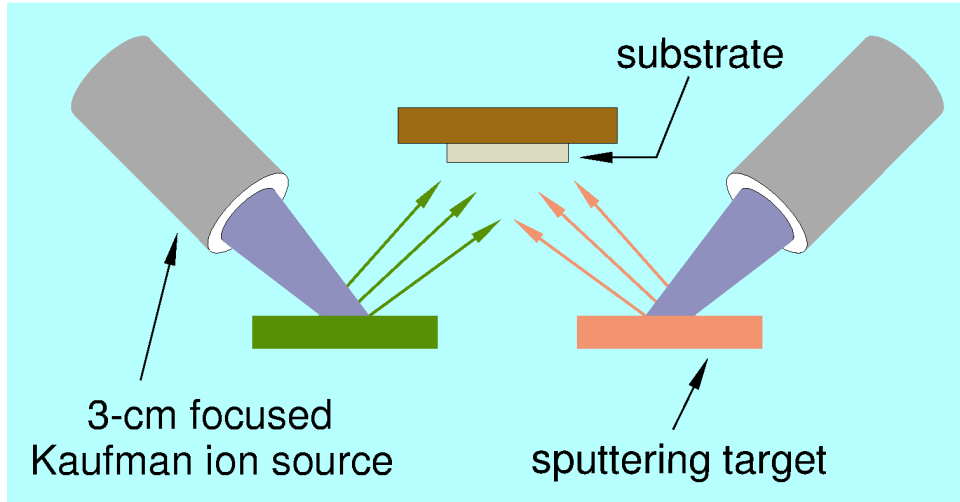


Figure 16. Schematic drawing of UHV ion beam sputtering system. Only two of the three Kaufman sputter ion sources are shown.

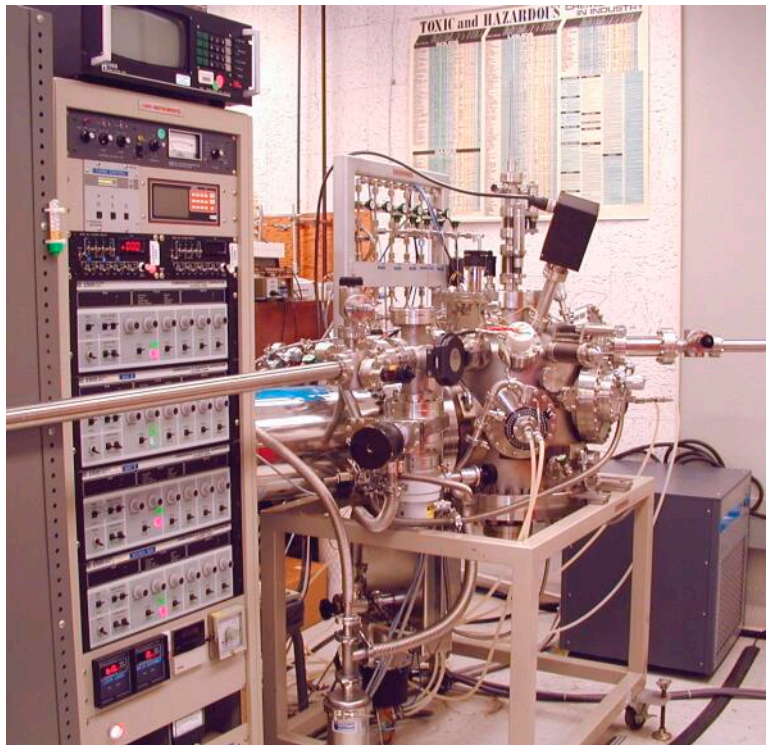


Figure 17. UHV ion beam sputtering system.

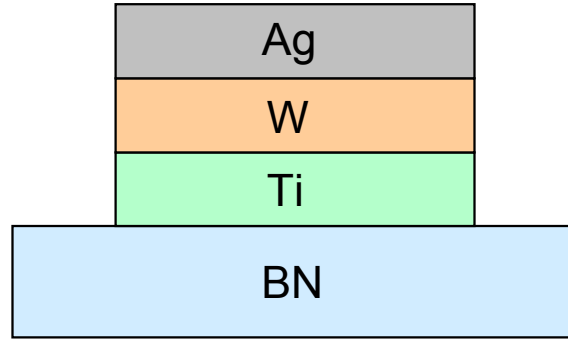


Figure 18. Deposition sequence of multilayer metal electrode.

A titanium nitride (TiN) layer was used in some cases as a combination diffusion-barrier/contacting layer in place of the tungsten-silver bilayer. The TiN layer was reactively sputtered in a partial pressure of N<sub>2</sub> gas immediately after the Ti layer deposition, using the same sputtering target. This approach has the following advantages:

- Fewer deposition steps (two electrode films instead of three)
- Reduced deposition system requirements (one sputtering target instead of three)
- Better film stability in subsequent furnace annealing step (Ag films agglomerate above 300°C)

### Electrode Patterning

The FIND device configuration shown in Figure 2 requires minimal or no patterning of the contact electrodes. However, to measure the contact properties, and for other possible electrode configurations (such as interdigitized top electrodes without a bottom electrode), a way of patterning the electrode metals is required. The approach used here is wet chemical etching after photolithographic pattern definition of the metal film trilayer or bilayer. See ELECTRODE ETCH RATES for the specific etchants used and their etch rates. The thickness of the FIND device electrodes was measured with a Veeco Dektak<sup>3</sup> ST profilometer after patterning.

## ELECTRICAL PROPERTIES CHARACTERIZATION

### Electrodes

The current-voltage and contact resistance properties of the multilayer metal film electrodes (see Electrode Deposition) were measured on electrodes patterned in various configurations. Fine silver wires were attached to the patterned electrodes using silver paint, as shown in Figure 19. Some electrical measurements were made *in-situ* as a function of temperature in a tube furnace in flowing argon gas. Figure 20 shows sample OUT77 mounted in the furnace test fixture (ready to be placed into the furnace).

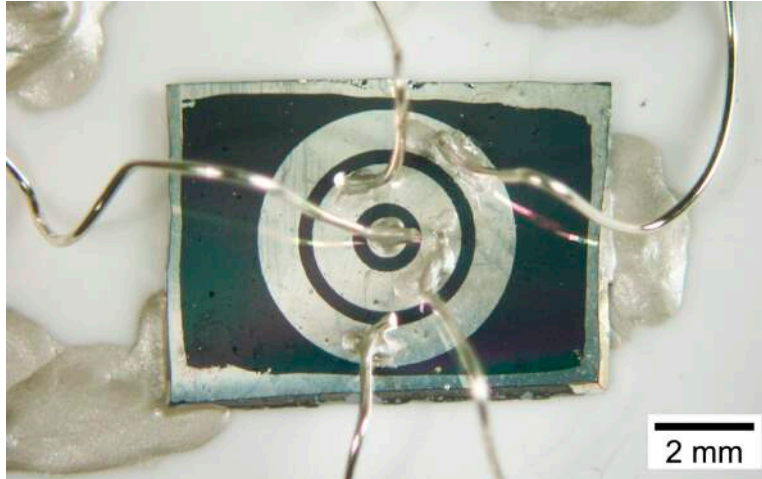


Figure 19. Silver wires connected to Ag/W/Ti electrodes on BN film sample OUT80.



Figure 20. BN film sample OUT77 mounted for *in-situ* furnace measurements.

### BN Films

The electrical resistance and current-voltage characteristics of the BN films provided by UMich were measured using the techniques described above. For the hBN film deposited on single crystal (100) MgO (sample OUT86), the current-voltage data were measured between two 0.5-mm-diameter Ag/W/Ti circular contacts, with 1.5 mm between contact centers. The BN film resistivity  $\rho$  was then extracted from these data using an expression for the measured resistance  $R$  of thin layers dominated by lateral current flow:<sup>16</sup>

$$R = \frac{\rho}{\pi d} \ln\left(\frac{s}{a}\right), \quad (16)$$

where  $d$  is the BN film thickness,  $s$  is the center-to-center separation distance between two circular contacts of radius  $a$ .

For hBN films deposited on semiconducting Si substrates, the BN resistivity was studied by four-probe van der Pauw measurements<sup>17,18</sup> of the film/substrate combination. For these measurements, small spots of indium were soldered to the corners on the back of the Si substrate. The resistivity of the BN film alone could not be measured directly because the conducting substrate can electrically short out the film (depending on the relative resistance of the film and the substrate). The resistivity of bulk hBN samples was determined from the current-voltage characteristic obtained using the corona discharge methods described above in CARRIER MOBILITY MEASUREMENTS.

## THERMAL NEUTRON DETECTION METHODS

The detecting element of the FIND device consists of a thin plate or film of boron nitride sandwiched between conducting electrode layers (that is, a capacitor structure). The electric field within the BN, due to the voltage applied across the device electrodes, collects any free charge generated by the nuclear reaction of Equation 1 that can reach the electrodes before being trapped or undergoing recombination. Each nuclear event (Equation 1) will therefore cause a sudden increase in the charge residing on the device electrodes. For low neutron flux densities, each increase will be discernable as a distinct charge pulse. An Amptek A250 charge sensitive preamplifier (see Figure 3) converts this charge pulse into a voltage pulse for subsequent display and processing.<sup>19</sup> The basic idea and advantages of a charge sensitive preamplifier are described in references 19 and 20.

The nuclear reaction rate  $\nu$  (Equation 8) is measured by counting the voltage pulses from the charge sensitive preamplifier. The pulses may be counted directly from the preamplifier (if large enough in amplitude and not overlapping), or from the output of a shaping circuit that amplifies and shapes the pulses to avoid “pile-up.”<sup>19</sup> The details of the amplifier circuit used here are given in Appendix A: CHARGE PULSE AMPLIFIER CIRCUIT. A photograph of the circuit, with cover removed, connected to the detector module (with sample OUT86 mounted in the center as a test neutron detection element) is shown in Figure 21.



Figure 21. Charge pulse amplifier with neutron detector module.



# RESULTS

## BORON NITRIDE FILM GROWTH AND STRUCTURAL CHARACTERIZATION

The following results were obtained by UMich using the methods described earlier. A number of hBN films were deposited under various growth conditions, mostly related to the grid voltage settings and N<sub>2</sub> gas flow rate for the Tectra ECR ion source. The initial films were grown with an N<sub>2</sub> flow rate of about 90 sccm, and ion source grid voltages on the order of 1 kV. Later films, grown after installing a gas-flow-limiting grid to the ion source, were deposited with an N<sub>2</sub> flow rate of 10 sccm and ion source grid voltages less than 100 V.

Figure 22 shows the RHEED images of a sample before and after growth of BN film SN021007. The growth conditions are listed in Table 3. A series of rings may be discerned in the RHEED image of the film after growth, indicative of the presence of polycrystalline BN.

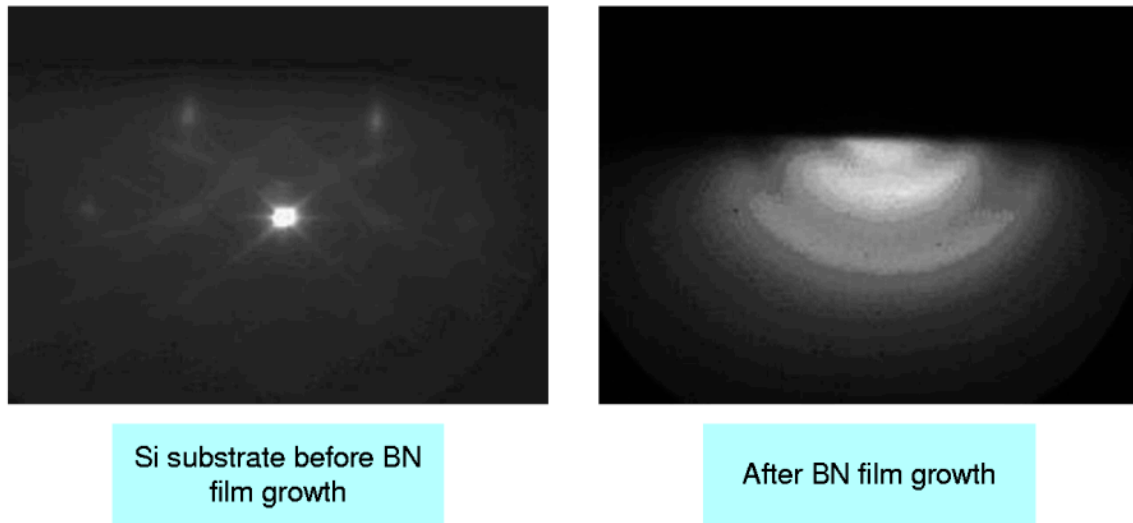


Figure 22. RHEED images before and after BN film SN021007 growth on (100) Si.

Table 3. BN film SN021007 deposition parameters.

Chamber pressure	5mTorr
Sputtering gun power	500 W Forward, 2 W Reflected
Substrate bias	-100 V
Substrate temperature	1000°C
ECR source anode voltage	1.2 kV
ECR source extractor voltage	-0.6 kV
ECR source magnetron current	55 mA
Growth Time	4.05 hrs

Figure 23 (background subtracted) was used to help identify the phase composition of the BN film. Transverse Optical (TO) phonon peaks were observed at  $1384\text{ cm}^{-1}$  and  $767\text{ cm}^{-1}$  (nominal values), indicative of the hexagonal phase.

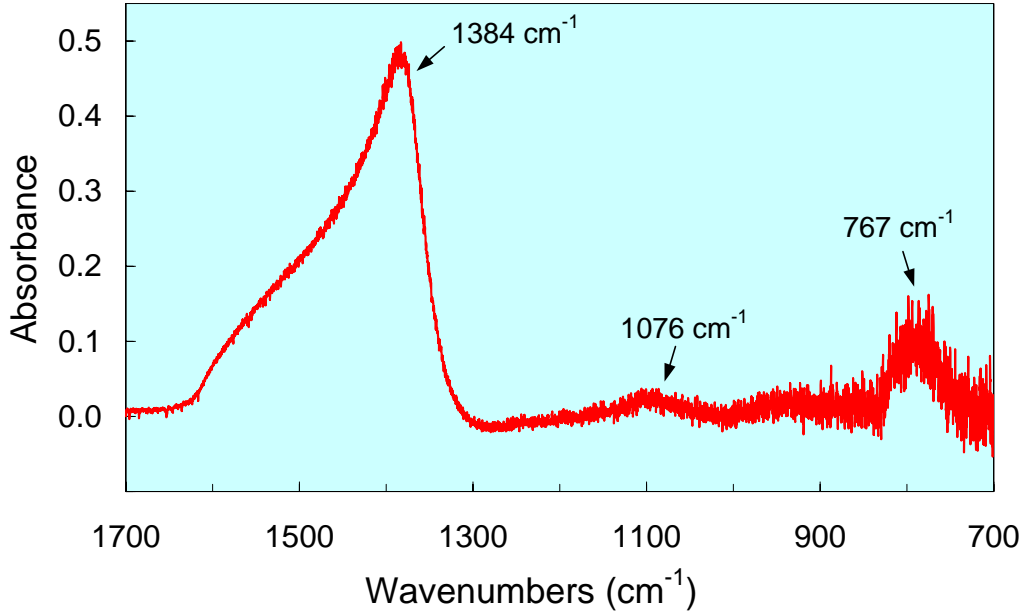


Figure 23. FTIR spectrum of BN film SN021007 deposited on (100) Si.

The x-ray diffraction spectrum of rather thick BN film (SN021118) deposited on (100) Si is shown in Figure 24. The growth conditions are listed in Table 4. From the  $\theta$ - $2\theta$  data of Figure 24, a correspondence was found between the theoretically calculated values and the experimentally obtained values for three diffraction peaks as listed in Table 5.

Table 4. BN film SN02118 deposition parameters.

Chamber pressure	5mTorr
Sputtering gun power	500 W Forward, 2 W Reflected
Substrate bias	-56 V
Substrate temperature	1000°C
ECR source anode voltage	1.2 kV
ECR source extractor voltage	-0.6 kV
ECR source magnetron current	55 mA
Growth Time	36 hrs

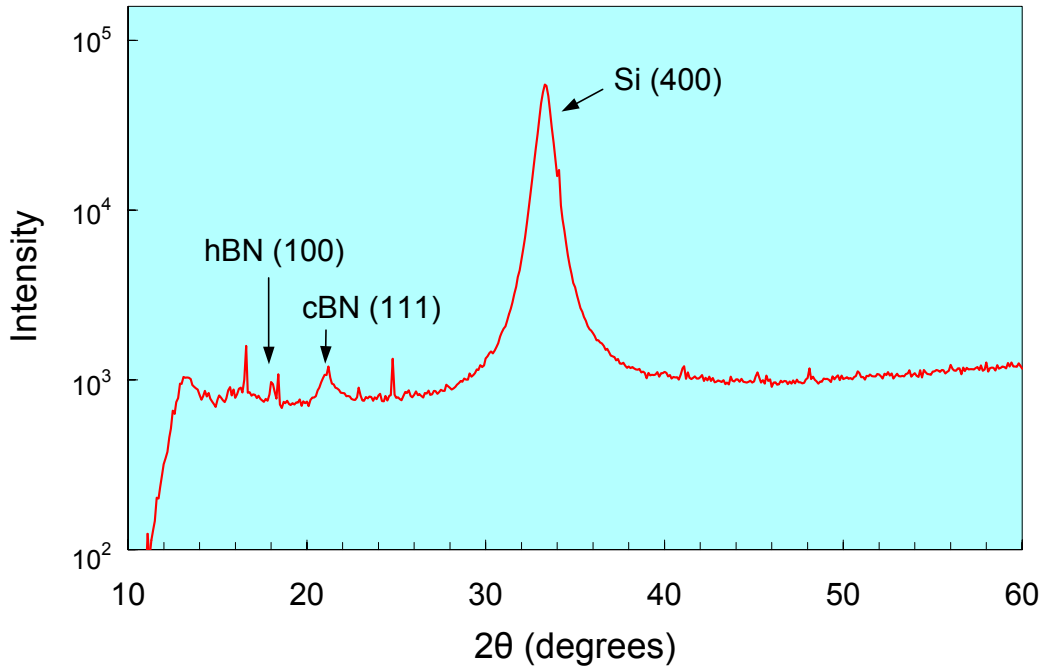


Figure 24. XRD spectrum of BN film SN021118 deposited on (100) Si.

Table 5. XRD peak comparison.

Peak	Theoretical Value 2θ (degrees)	Experimental Value 2θ (degrees)
Si (400)	33.21002	33.30191
h-BN (100)	17.82588	17.99931
c-BN (111)	21.42565	21.19911

Thus, from the XRD data, the boron nitride film contains crystalline cBN and hBN phases. The size of the domains may be estimated by considering the width of the diffraction peaks of Figure 24. Based on this analysis, the grain size of (100) hBN is about 20 nm, and that of (111) cBN is approximately 7 nm. Scanning electron micrographs of the BN film are shown in Figure 25, with the Si substrate positioned above the BN film. The photograph on the right, showing a BN film thickness of about 3.6 μm, is at a much higher magnification than that on the left.

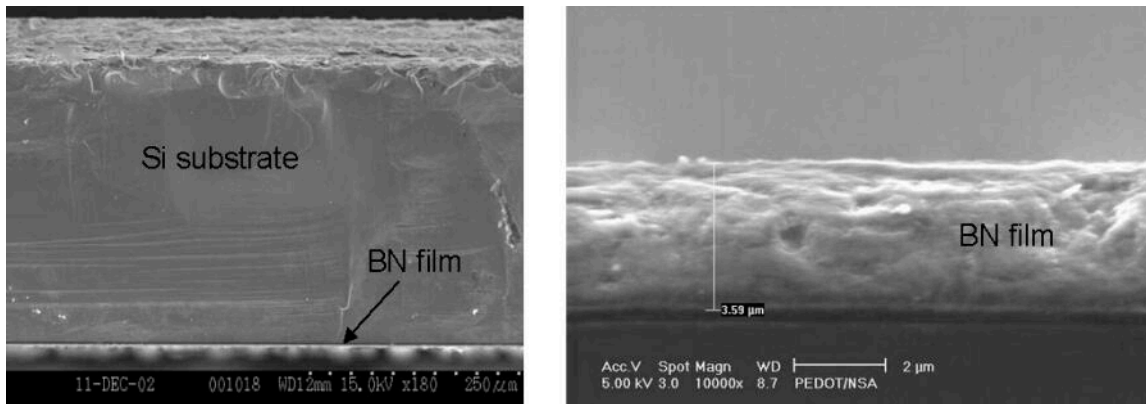


Figure 25. SEM photographs of BN film SN021118 deposited on (100) Si.

Another thick BN film (SN030125), grown under the conditions given in Table 4, was deposited on a (100) MgO substrate. A photograph of one portion of this film is shown in Figure 26. The FTIR spectrum of another portion of the film is shown in Figure 27. Only the hBN peak at  $1390\text{ cm}^{-1}$  is observed, not the cBN peak at  $1076\text{ cm}^{-1}$ .

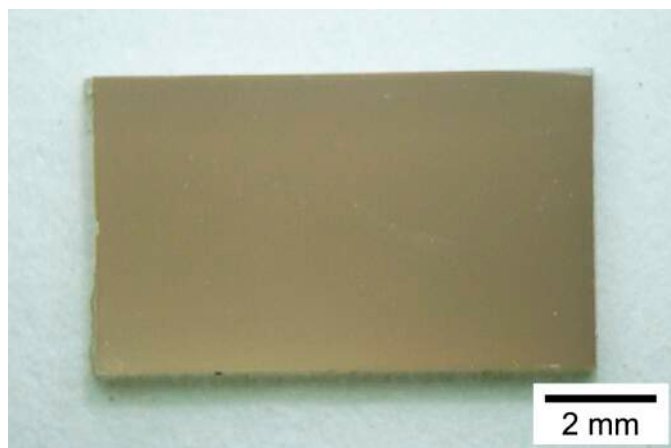


Figure 26. Hexagonal BN film sample OUT81 on (100) MgO. This sample was cut from parent sample SN030125.

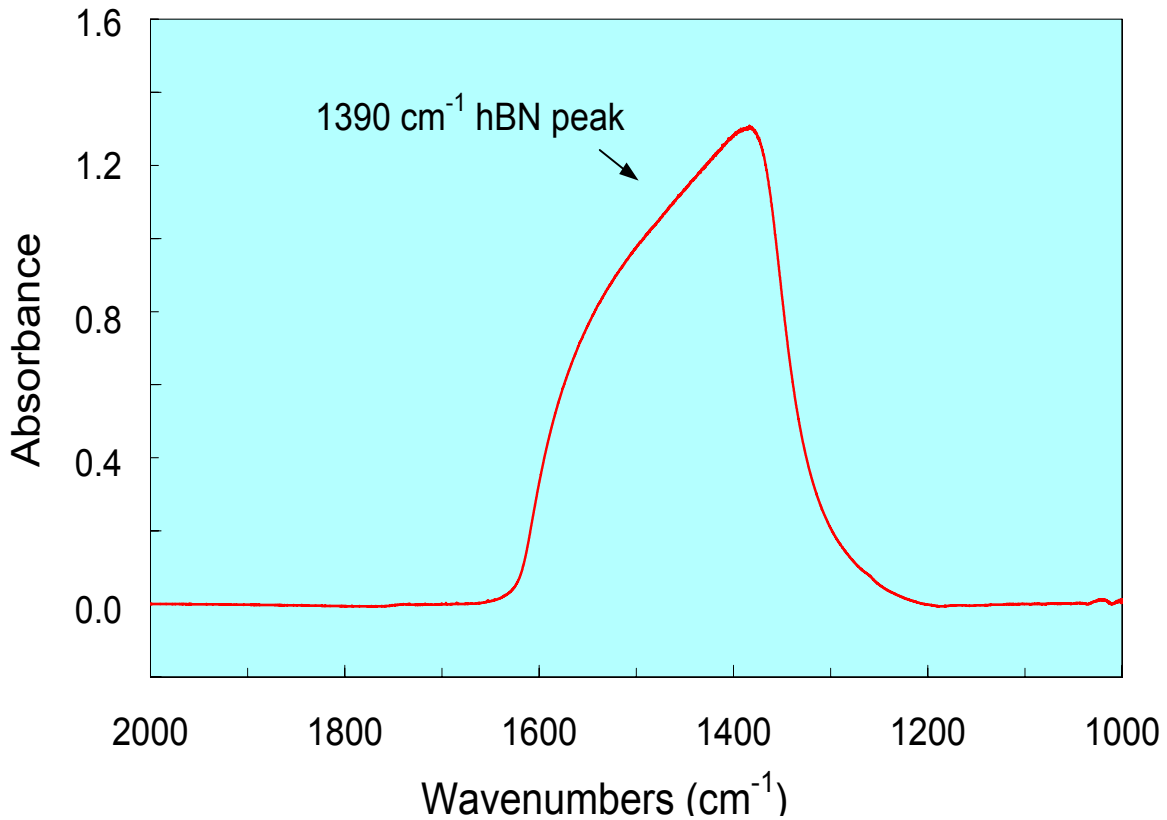


Figure 27. FTIR spectrum of BN film SN030125 on (100) MgO.

After modifying the ECR ion source to reduce the  $N_2$  gas flow, a series of BN films were deposited on (100)-oriented high-resistivity ( $5000 \Omega\text{-cm}$ ) Si. These films were deposited at reduced nitrogen ion energies. The FTIR spectrum of one of these films (SN030813), shown in Figure 28, indicates that the crystalline phase of the film is purely hexagonal (no cubic phase). The growth conditions for this film are given in Table 6.

Table 6. Reduced gas glow sample deposition parameters.

Chamber pressure	5mTorr
Sputtering gun power	502 W Forward, 2 W Reflected
Substrate bias	-96.6 V
Substrate temperature	1000°C
ECR source anode voltage	80 V
ECR source extractor voltage	-40 V
ECR source magnetron current	65 mA
Growth Time	8.33 hrs

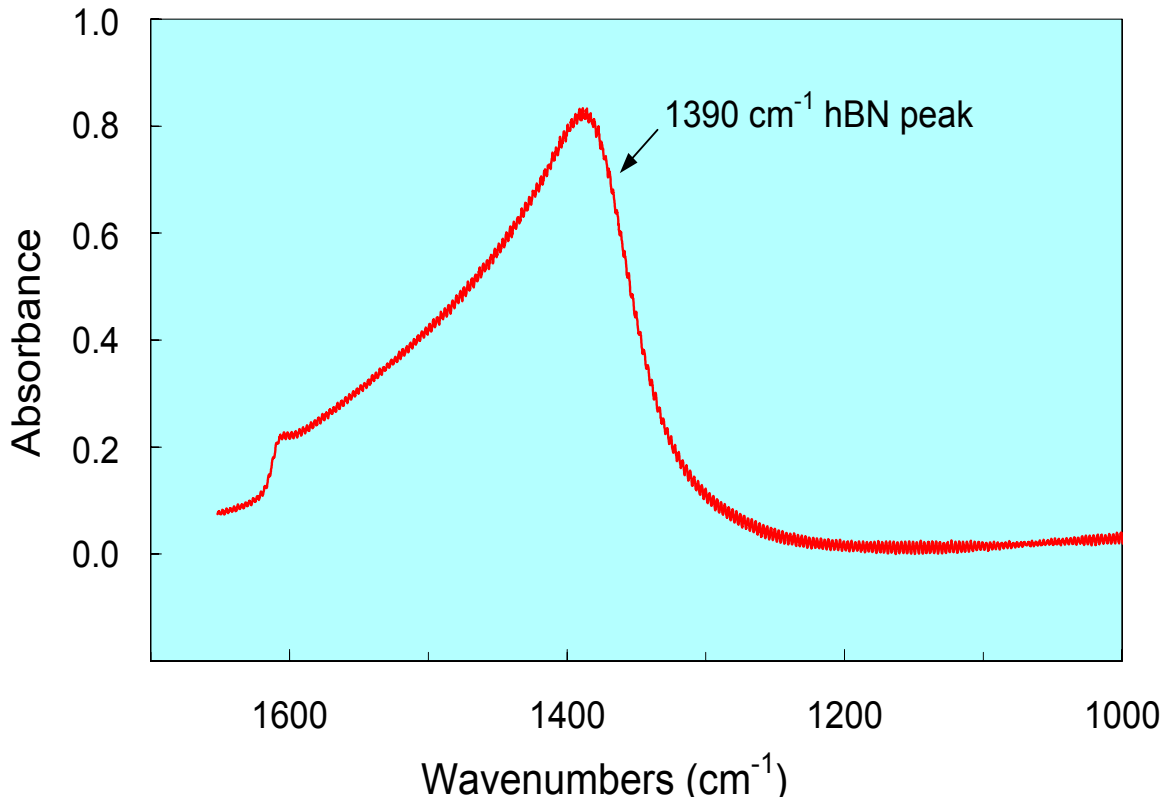


Figure 28. FTIR spectrum of BN film SN030813 on (100) high-resistivity Si.

## CARRIER LIFETIME MEASUREMENTS

### Microwave Cavity Perturbation

The following results were obtained by VCU using the microwave cavity perturbation (MCP) technique. Three hBN film samples, grown on single crystal (100) MgO substrates and with a bandgap of roughly 5.8 eV,<sup>21</sup> were provided by UMich as cut from film sample SN030125. A bare (100) MgO sample was also supplied by UMich for comparison purposes. Bulk hBN samples (BLK10 and BLK11), manufactured as Combat<sup>®</sup> AX05 grade by The Carborundum Company (now the Saint-Gobain Advanced Ceramics Corporation), were also provided to VCU by SSC San Diego. Both sets of samples were evaluated as received; no sample preparation of any kind was performed.

For all samples, the laser excitation wavelength was varied from the fundamental of a Nd:YAG laser (1064 nm) to the three harmonics (532, 355, and 266 nm). All incident wavelengths are sub-band to the BN bandgap for all samples (that is, the laser energy is less than the sample bandgap energy). A bare MgO substrate showed no response at all wavelengths at room temperature or at liquid nitrogen temperature. One of the hBN films grown on MgO produced the room temperature response shown in Figure 29.

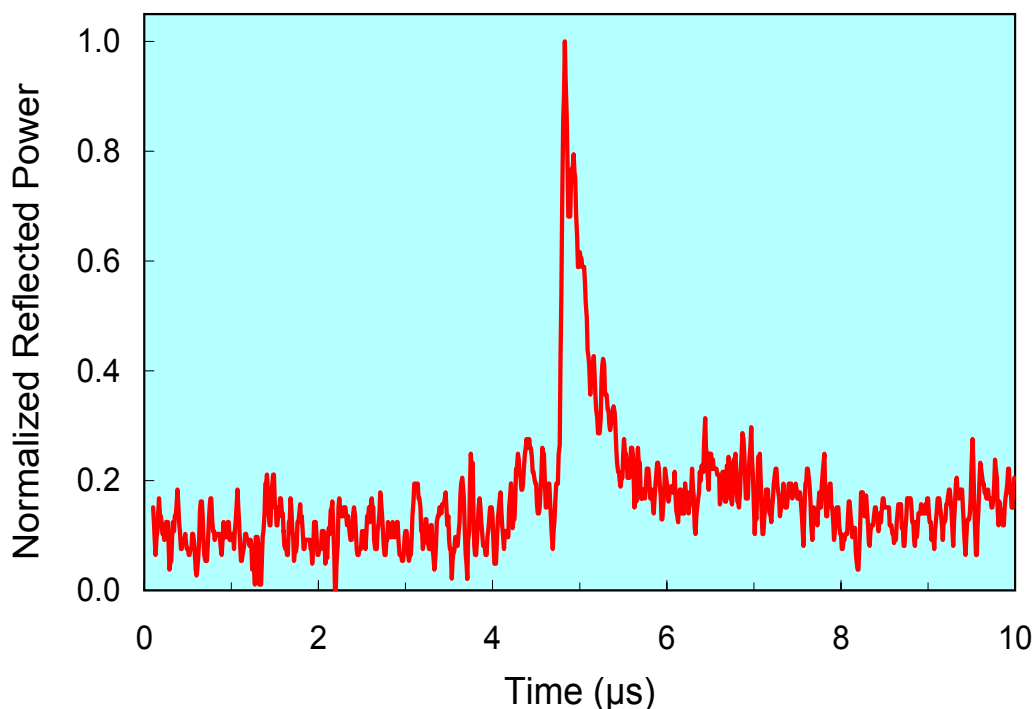


Figure 29. Response of hBN film SN030125 on MgO using the MCP technique.

These data were generated with a laser wavelength of 532 nm, laser energy of 25 mJ/pulse, pulse width of 6 nS, and a pulse repetition rate of 10 Hz. Ablation of the sample was apparent after the experiment. The remaining samples of hBN on MgO showed no response when placed under similar conditions. These very aggressive lasing conditions were necessary to obtain the signal shown in Figure 29, but the results were not reproducible. Assuming that the Figure 29 data are valid, however, analysis of the type shown in Figure 10 gives a carrier lifetime of 360 ns for this hBN film on MgO.

The bulk hBN samples received from SSC San Diego were also examined under the room temperature lasing conditions described above, as well as at liquid nitrogen temperature. No response was observed for these samples, but surface ablation did occur.

Both the film and bulk hBN samples are essentially insulating materials with very large bandgaps. For a high-purity sample, or one with deep-level impurities, the above results may be due to an excitation wavelength that is too large to excite electrons (or holes) into the conduction (or valence) band. The results may also be due to a high number of impurities or lattice defects, both of which can act as charge carrier traps, leading to low carrier lifetime. If the carrier lifetime is below about 100 ns, it cannot be accurately measured using this microwave technique.

It is therefore possible that higher energy photons are necessary for measuring the carrier lifetime. This assertion can be supported by the identification of defect levels in hBN at 3.40, 3.84, 4.40, 4.90, 5.31, and 5.50 eV. The nature of these defects is unclear, but their existence is shown by UV emission in reference 21. It may be necessary to use photons with energies of at least 5.6 eV (~225 nm wavelength), beyond the deepest reported defect energy level.<sup>21</sup>

### Time-Resolved Reflectivity

Initial time-resolved reflectivity (TRR) measurements at UMich on hBN/MgO sample SN030125 gave a null result using a laser wavelength of 800 nm. Higher energy illumination may be needed because of the high-energy bandgap of BN, or because any traps may be too deep in the bandgap for this wavelength. A new reflectivity apparatus is being set up at UMich that is capable of using frequency doubling or tripling crystals (corresponding to wavelengths of 400 and 266 nm, respectively) to obtain higher laser energy.

### CARRIER MOBILITY MEASUREMENTS

Using the corona discharge method described in CARRIER MOBILITY MEASUREMENTS and illustrated in Figure 15, current versus voltage measurements were made on a thinned piece of bulk hBN with a thickness of 0.4 mm. The sample surface was exposed to the discharge through a circular opening (with an area of 0.85 cm<sup>2</sup>) in the ground shield. A multilayer metal electrode, as shown schematically in Figure 18, had been deposited on the opposite side of the sample and grounded. The results of this measurement on sample BLK12 are shown in Figure 30.

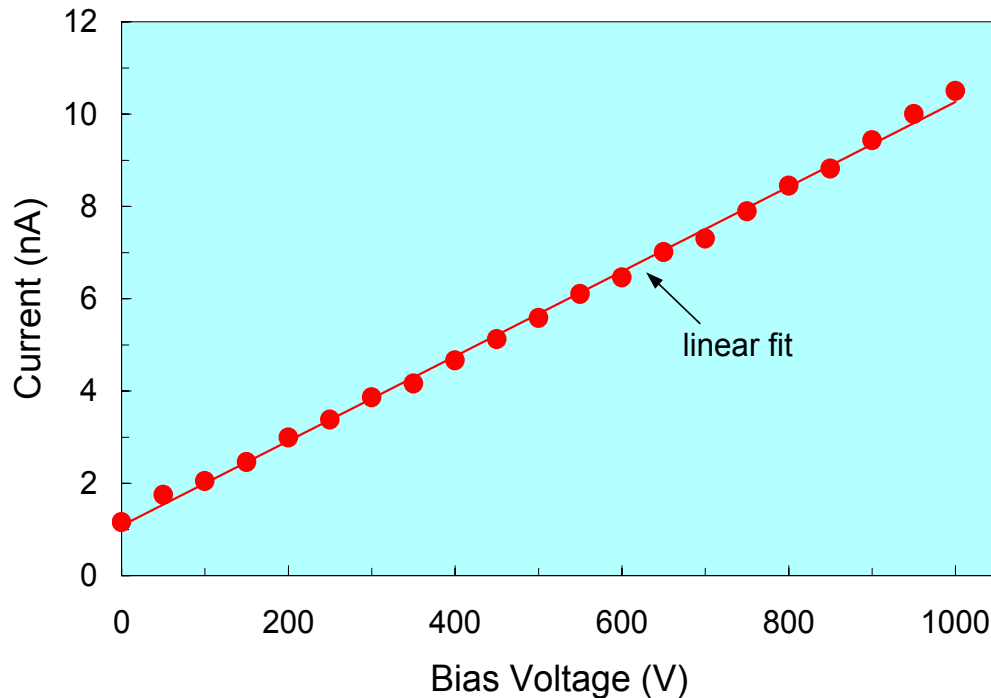


Figure 30. Sample current versus bias voltage for hBN bulk sample BLK12.

The linear current-voltage characteristic observed here, described by Equation 15, indicates that charge conduction in this sample is not space charge limited. Therefore, the carrier mobility  $\mu$  cannot be determined from Equation 14. Equation 15 could be used to calculate  $\mu$ , but the carrier density  $n$  of this sample is not known. Measurement of the carrier density (using, for example, a Hall effect method) in very high-resistance, wide-bandgap materials such as BN is extremely difficult. Films of BN will likely be more amenable to corona discharge methods of determining the mobility (just as for polymer films) because higher electric fields can be achieved (for a given surface potential) due

to the smaller thickness of films compared to bulk samples. Thinned bulk hBN samples are limited to a thickness of about 400  $\mu\text{m}$ , below which they tend to lose structural integrity (i.e., they crumble).

## ELECTRODE ETCH RATES

As discussed in Electrode Patterning, the electrode metals for the FIND device were patterned using wet chemical etching. Different etching solutions are needed for different metals, and the etchant must not attack (dissolve) the photoresist (Shipley S1813) during the etching process. A number of possible etchants, listed in Table 7, were tested. The first chemical listed in etch 7 is ethylenediaminetetraacetic acid (EDTA).

Table 7. Electrode metal wet etchants.

Metals	Etchant number	Etchant chemicals	Amounts	Etch rate ( $\mu\text{m}/\text{min}$ )	Comments
Ag, W	1	ammonium hydroxide hydrogen peroxide methanol	1 ml 1 ml 4 ml	not measured	dissolved photoresist
Ag	2	ammonium hydroxide hydrogen peroxide water	1 ml 1 ml 4 ml	15.4	
W	3	potassium hydroxide potassium phosphate monobasic potassium ferricyanide water	340 mg 134 mg 330 mg 10 ml	not measured	dissolved photoresist
W	2	ammonium hydroxide hydrogen peroxide water	1 ml 1 ml 4 ml	5.3	
Ti	4	hydrofluoric acid hydrogen peroxide water	1 ml 1 ml 20 ml	8.9	lifted BN film from MgO substrate
Ti	5	hydrofluoric acid glycerine	1 ml 20 ml	0.033	stir well
TiN	6	ammonium hydroxide hydrogen peroxide water	1 ml 6.6 ml 21.9 ml	0.005	heated to 35°C; Ref. 22
TiN	7	EDTA hydrogen peroxide water	15 mg 16.6 ml 33.4 ml	0.005	heated to 65°C

Etchant 5 was used for sample SN030125 (BN film on MgO substrate; see Figure 26) because it was found that etchant 4 (specifically, the water in the etchant) caused the BN film of this sample to separate from the substrate. This separation may be due to the possible formation of water-soluble boric oxide,  $\text{B}_2\text{O}_3$ , or similar compounds at the film-substrate interface during film growth at 1000°C, perhaps because of a reaction of BN with MgO at this elevated temperature.

## ELECTRICAL PROPERTIES

### Electrodes

As described in ELECTRICAL PROPERTIES CHARACTERIZATION/Electrodes, the temperature-dependent resistance and current-voltage characteristics of Ag/W/Ti electrodes (see Figure 18), deposited on either cBN or hBN films on silicon substrates, were measured. The time dependence of the resistance between two such contacts on cBN/Si sample OUT71, as well as that of the sample temperature during furnace processing, is shown in Figure 31.

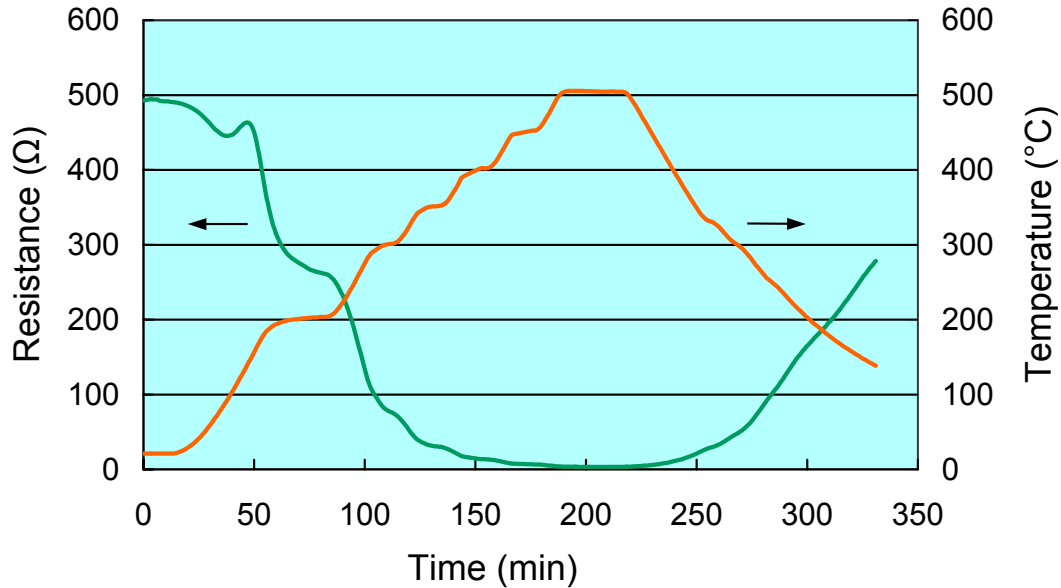


Figure 31. Furnace cycle for Ag/W/Ti contacts on cBN-Si sample OUT71.

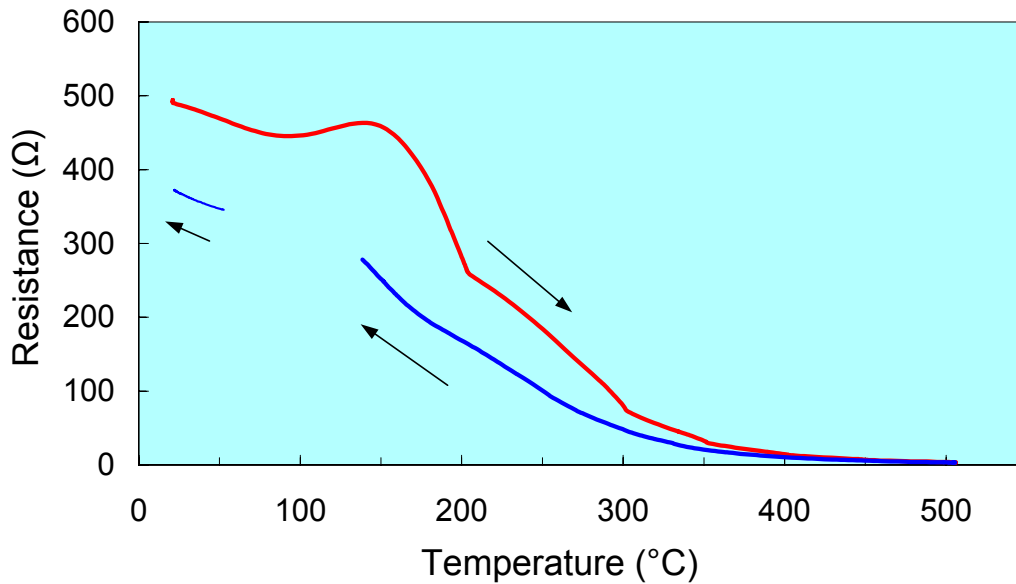


Figure 32. Resistance between contacts versus temperature for cBN-Si sample OUT71.

The resistance data of Figure 31 are also shown in Figure 32 as a function of temperature. Note that the resistance measured during the cooling cycle is lower than that during the heating cycle. Because the measured resistance is a combination of contact and film resistances, and the film resistance is not expected to change significantly by processing in this temperature range (for that part of the film not close to the contact/film boundary), this resistance drop can be attributed to a lowering of the contact resistance, presumably due to Ti-B and Ti-N reaction at the Ti/BN interface. The gap in the cooling data is most likely due to one of the silver wires being temporarily pulled away from the sample because of thermal stresses on the wires.

### BN Films

Using the techniques described in ELECTRICAL PROPERTIES CHARACTERIZATION/BN Films, resistance and current-voltage (I-V) measurements were made between two multilayer metal electrodes deposited on either cBN or hBN films. The room temperature I-V characteristics for hBN film OUT86 (cut from sample SN030125) is shown in Figure 33. The film resistance (including any contact resistance) and resistivity derived from these data are shown in the figure. For the resistivity calculation, the contact resistance is assumed to be small compared to the film resistance.

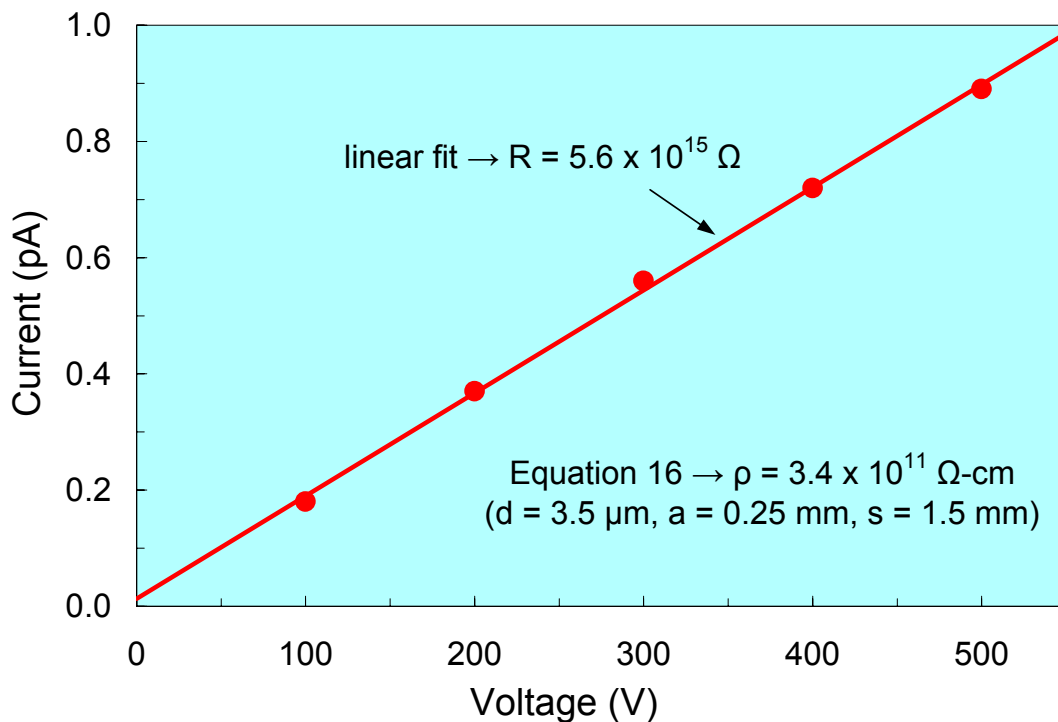


Figure 33. I-V characteristic between circular contacts on hBN/MgO sample OUT86.

For hBN bulk sample BLK12, a linear fit to the data of Figure 30 gives a sample resistance of  $1.1 \times 10^{11} \Omega$ . Using the geometric parameters given above for this sample in CARRIER MOBILITY MEASUREMENTS, the resistivity of BLK12 is  $2.3 \times 10^{12} \Omega\text{-cm}$ .

## THERMAL NEUTRON DETECTION RESULTS

A test detector using bulk hBN sample BLK13 sputter-coated with top and bottom TiN/Ti electrodes is shown in Figure 34. The average thickness of this sample is 0.2 mm, and the detection area (top electrode area) is 56 mm<sup>2</sup>. The current pulse count rate of this test device was measured as a function of bias voltage across the sample (see Figure 35) using the charge pulse amplifier circuit and instrumentation described earlier in THERMAL NEUTRON DETECTION METHODS. The readings were taken both with and without the Am-Be neutron source near the sample. Low-density polyethylene, 2.0 cm thick, and lead sheet, 1.3 cm thick, were placed between the detector and the source. The polyethylene thermalizes any fast neutrons going toward the detector from the source (increasing the flux of thermal neutrons, which are more likely to interact with the BN than more energetic neutrons). The lead shields the detector from gamma rays coming from the source (in order to see only the effect of the neutrons on the detector). Note that this result, clear and unambiguous at the time, could not be repeated in measurements performed several weeks later, perhaps due to oxidation of the titanium electrodes.

Although high-resistivity BN films, required for a film-based FIND device, have been produced in this effort (see Figure 33), such films have not yet been deposited with a bottom metallic electrode (required for the desired capacitor device structure). An alternate electrode configuration using interdigitized top-only electrodes on hBN film sample OUT86 (cut from parent sample SN030125; deposited on an insulating MgO substrate) was tried in the interim, as shown in Figure 36. Note that this is a far from optimal electrode configuration because the electric field produced with this arrangement is mainly at the BN film surface; the full field does not completely penetrate through the film thickness as it would in a capacitor configuration. It is not surprising, therefore, that neutron detection measurements (as described above for the bulk hBN test detector) yielded a null result.

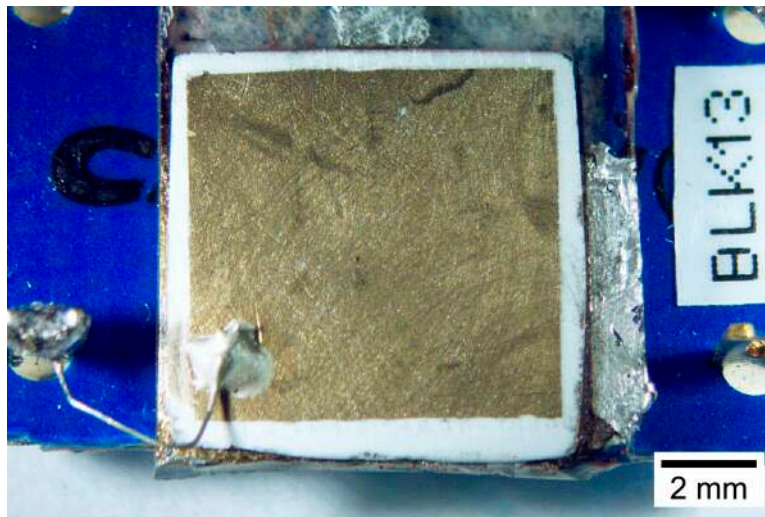


Figure 34. Bulk hBN sample BLK13 in FIND configuration.

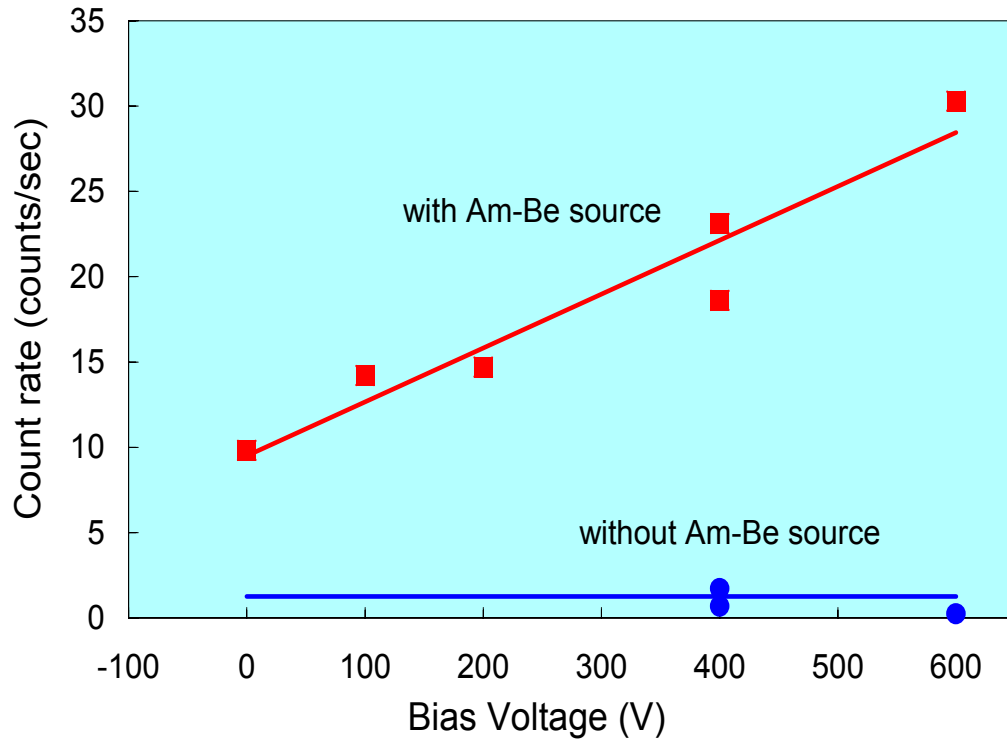


Figure 35. Charge pulse count rate for bulk hBN sample BLK13.

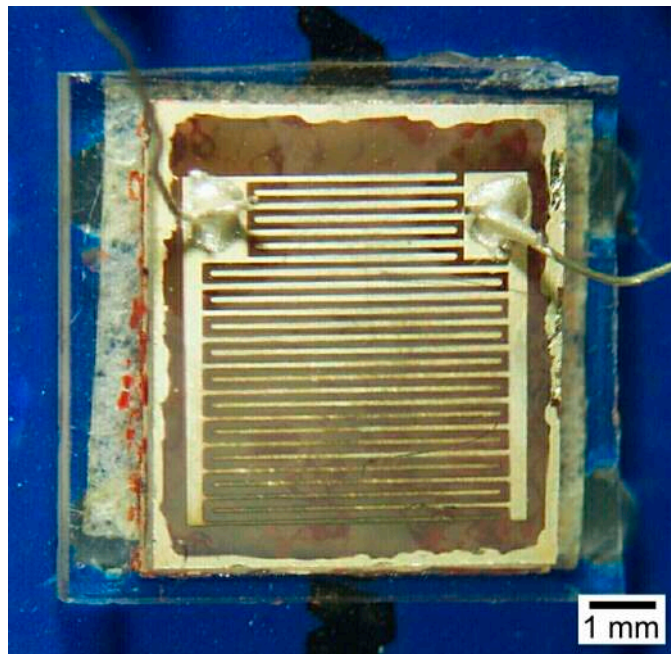


Figure 36. Hexagonal BN film sample OUT86 on MgO with interdigitized electrodes.



## SUMMARY AND CONCLUSIONS

A proof-of-concept FIND device with a thin bulk BN detecting element has been demonstrated to be sensitive to irradiation by thermal neutrons. The neutron reaction count rate was seen to increase linearly with the bias voltage applied across the BN thickness. This dependence indicates that the fraction of the BN participating in the detection process is limited by the mobility-lifetime product  $\mu\tau$  of the free carriers generated in the neutron-boron reaction. Measurement of  $\mu$  and  $\tau$  (or the  $\mu\tau$  product) is therefore critical both as a sample evaluation tool (i.e., will a given sample work as a detecting element?) and as an indicator of sample properties and characteristics that need improvement (e.g., grain boundary density, impurity doping level, etc.).

Various methods for measuring these key BN properties, as well as ways of characterizing the electrical contacts to the material, have been investigated for both thin film and bulk samples of hexagonal-phase boron nitride. The structural properties of cBN and hBN films grown by magnetron sputtering in a UHV system have been examined using reflection high-energy electron diffraction, scanning electron microscopy, Fourier transform infrared spectroscopy, and x-ray diffraction. Most of the films were deposited on Si substrates; one hBN film was grown on MgO.

A non-contact technique, microwave cavity perturbation, was used to measure the carrier lifetime  $\tau$  of the hBN film on MgO and of bulk hBN. For the most part, no response was seen after laser excitation of the samples. In one case, extreme illumination of the hBN film sample produced a response that gives a carrier lifetime value of 360 ns. For the measured film resistivity of  $3.4 \times 10^{11} \Omega\text{-cm}$ , a minimum carrier mobility of about 1 V/(cm-s) would be required for this sample to work as the detecting element in a FIND device. This film, however, was deposited on an insulating substrate, and so could not be configured with a bottom conducting electrode, the preferred FIND configuration. Neutron detection measurements with interdigitized electrodes on the film's top surface gave a null result.

Because of the low carrier lifetimes of currently available samples indicated by the microwave cavity perturbation technique, another method of measuring the lifetime was investigated. The time-resolved reflectivity method has a time-resolution of approximately 200 fs. Initial measurements of the hBN on MgO film indicated that the excitation laser energy is not high enough to promote carriers (whose lifetime is to be measured) into the hBN conduction band. Higher energies will be obtained using doubling or tripling crystals.

Because of the difficulty of measuring the carrier mobility of high-resistivity samples using standard techniques (such as Hall effect measurements), a corona discharge method of determining the carrier drift mobility from the time-dependent build-up or decay of a surface voltage was investigated. Under constant-current space-charge-limited conditions, the mobility is related in a simple way to the initial time rate of change of the surface voltage, the steady-state surface voltage, and the sample geometry. Initial measurements of the current-voltage characteristics of bulk hBN samples show, however, that charge conduction in this relatively thick sample is not space charge limited in the voltage range used. BN films, or thinner bulk samples, will be more amenable to this method of determining the mobility because higher electric fields can be achieved for a given surface potential.

In order to perform the key materials property measurements described above, and to configure the BN detecting element as a FIND device, a number of sample preparation and characterization steps have also been studied and implemented, including:

- hBN film growth conditions
- Highly visual approach for substrate selection for epitaxial film growth
- Deposition of reactive/diffusion-barrier/contacting multilayer metal electrodes
- Wet etching techniques for multilayer metal electrode patterning
- *In-situ* furnace measurements of resistance between contacts
- Transmission line methods for specific contact resistivity measurements
- Current pulse amplifier design and construction for neutron detection testing

## RECOMMENDATIONS FOR FURTHER DEVELOPMENT

The successful operation of a bulk BN thermal neutron detector affirms the basic concept of the FIND device. Further work is needed to make a reproducible and reliable detector, and to incorporate and optimize a high quality BN film detection element that would have the following advantages:

- Thinner than typical bulk material → low bias voltage (not kilovolts)
- Fewer structural defects → higher charge carrier lifetime → higher detection efficiency
- Lower porosity level → more nuclear reactions in given volume → higher detection efficiency

An alternative to a BN film detection element is very thin, robust, highly oriented bulk BN (including single crystal BN, when BN crystal growth is at an advanced enough stage).

In any case, successful implementation of a FIND device will require the continued refinement and use of methods for measuring the carrier mobility  $\mu$  and lifetime  $\tau$  (or the lifetime-mobility product  $\mu\tau$ ) of the BN detecting element. Measurement of the specific resistivity and chemical/ structural properties of the device electrical contacts is also crucial. Characterization of these BN and contact properties will be essential for screening and improving FIND devices, and ultimately for quality control.



## REFERENCES

1. J. Losee, J. C. Hicks, E. W. Jacobs, W. C. McGinnis, and R. D. Boss, "Boron Nitride Solid State Detector for Thermal Neutrons," U.S. Patent Disclosure, Navy Case No. 83098 (2001).
2. K. Hermann, LATUSE Ver. 4.0, <http://w3.rz-berlin.mpg.de/~hermann/SLP/>, Fritz-Haber-Institut, Germany (1994).
3. D. Litvinov and R. Clarke, "Reduced Bias Growth of Phase-Pure Cubic Boron Nitride," *Appl. Phys. Lett.* **71**, 1969 (1997).
4. S. M. Sze, *Physics of Semiconductor Devices*, 2<sup>nd</sup> ed. (John Wiley & Sons, New York, 1981), Sec. 1.7.2, p. 52.
5. D. J. Harris and P. N. Robson, *The Physical Basis of Electronics* (Permagon Press, Oxford, 1974), Sec. 9.1.1, p. 168.
6. G. F. Leal Ferreira and M. T. Figueiredo, "Corona Charging of Electrets," *IEEE Trans. Elect. Insul.* **27**, 719 (1992).
7. J. A. Giacometti and J. S. Carvalho Campos, "Constant Current Corona Triode with Grid Voltage Control. Application to Polymer Foil Charging," *Rev. Sci. Instrum.* **61**, 1143 (1990).
8. M. A. Lampert and P. Mark, *Current Injection in Solids* (Academic Press, New York, 1970), Ch. 4, p. 45.
9. M. J. Russ, "Surface Conduction in Group II-VI Semi-Insulators," *J. Appl. Phys.* **34**, 1831 (1963).
10. I. P. Batra, K. K. Kanazaw, and H. Seki, "Discharge Characteristics of Photoconducting Insulators," *J. Appl. Phys.* **41**, 3416 (1970).
11. See, for example, Y. Eisen, A. Shor, and I. Mardor, "CdTe and CdZnTe Gamma Ray Detectors for Medical and Industrial Imaging Systems," *Nucl. Instrum. Methods A* **428**, 158 (1999).
12. W. E. Spear, "Transit Time Measurements of Charge Carriers in Amorphous Selenium Films," *Proc. Phys. Soc. London, Sect. B*, **70**, 669 (1957).
13. E. H. Martin and J. Hirsch, "Electron-Induced Conduction in Plastics. I. Determination of Carrier Mobility," *J. Appl. Phys.* **43**, 1001 (1972).
14. K. L. Moazed, J. R. Ziedler, and M. J. Taylor, "A Thermally Activated Solid State Reaction Process for Fabricating Ohmic Contacts to Semiconducting Diamond," *J. Appl. Phys.* **68**, 2246 (1990).
15. W. C. McGinnis, "Electronic Properties of Cubic Boron Nitride," in *ILIR '00: SSC San Diego In-House Laboratory Independent Research Annual Report*, SSC San Diego Technical Report **3115**, 94 (May 2001).
16. D. H. Dickey and J. R. Ehrstein, *Spreading Resistance Analysis for Silicon Layers with Nonuniform Resistivity*, NBS SP **400-48** (1979).

17. L. J. van der Pauw, "A Method of Measuring Specific Resistivity and Hall Effect of Discs of Arbitrary Shape," *Philips Res. Rpts.* **13**, 1 (1958).
18. L. J. van der Pauw, "A Method of Measuring the Resistivity and Hall Coefficient of Lamellae of Arbitrary Shape," *Philips Tech. Rev.* **20**, 220 (1959).
19. K. Kobayashi, *Development of a Balloon-borne Hard X-ray Spectrometer for Solar Flare Observation*, M.S. thesis, University of Tokyo (2000).
20. S. Buchman, J. Mester, and T. J. Sumner, in *The Measurement, Instrumentation, and Sensors Handbook*, edited by J. G. Webster (CRC Press, Boca Raton, FL, 1999), Chap. 44.
21. C. A. Taylor, S. W. Brown, V. Subramaniam, S. Kidner, S. C. Rand, and R. Clarke, "Observation of Near-Band-Gap Luminescence from Boron Nitride Films," *Appl. Phys. Lett.* **65**, 1252 (1994).
22. S. Verhaverbeke and J. W. Parker, "A Model for the Etching of Ti and TiN in SC-1 Solutions," in *Science and Technology of Semiconductor Surface Preparation, San Francisco, 1997, Materials Research Society Symposium Proceedings Series 477*, 447, edited by G. S. Higashi, M. Hirose, S. Raghavan, and S. Verhaverbeke (Materials Research Society, Pittsburgh, 1997).

## APPENDIX A: CHARGE PULSE AMPLIFIER CIRCUIT

The details of the charge pulse amplifier of Figure 3 are shown in Figures A-1 and A-2.

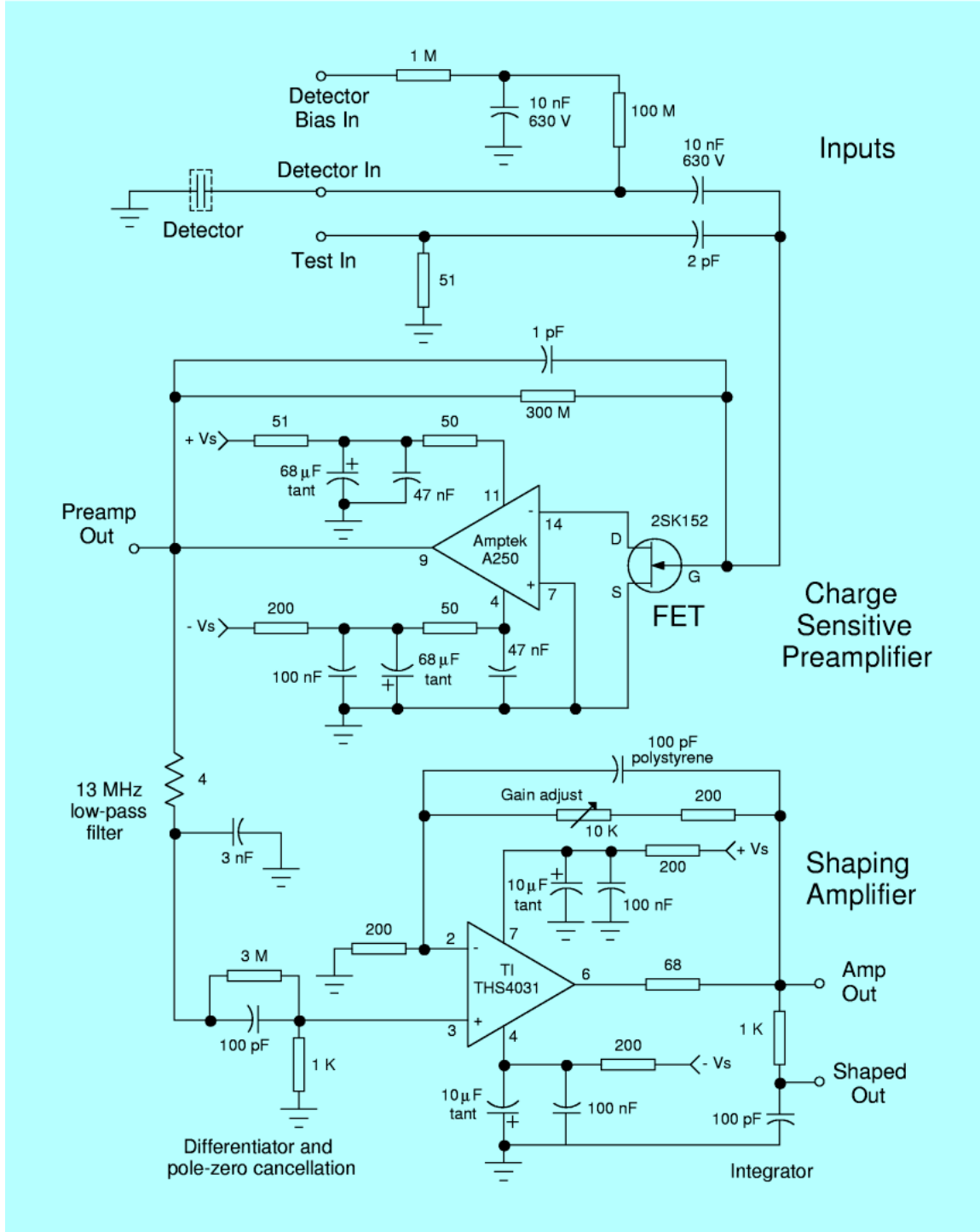


Figure A-1. Charge pulse amplifier circuit.

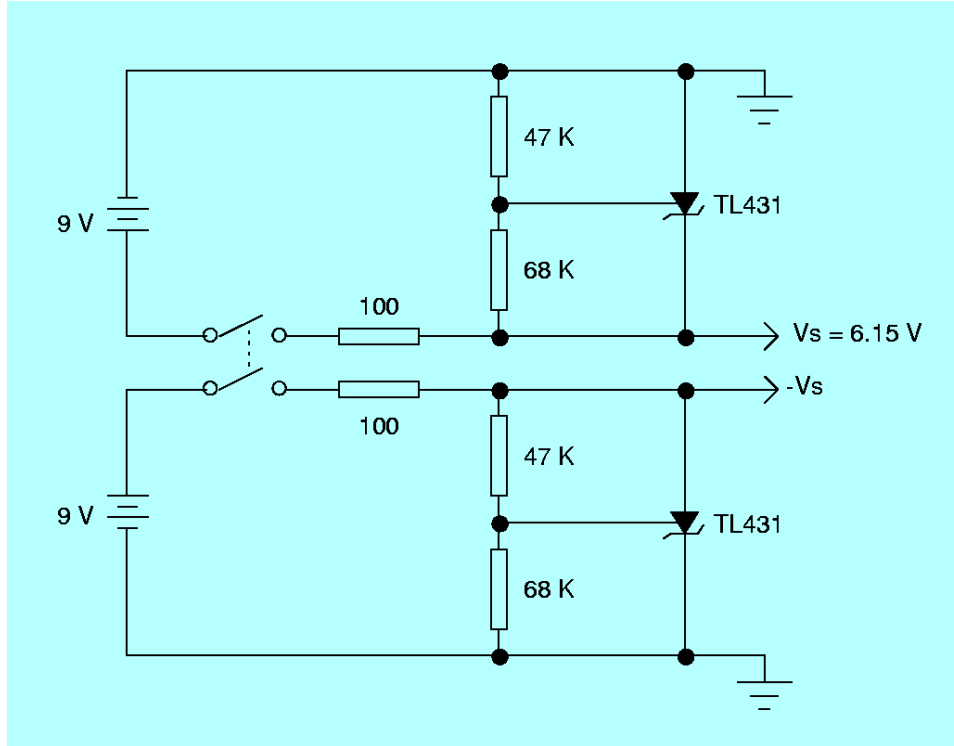


Figure A-2. Power supply circuit for charge pulse amplifier of Figure A-1.

The Amptek A250 charge sensitive preamplifier of Figure A-1 converts the charge pulse produced in the FIND device (detector) by the neutron-boron nuclear reaction (Equation 1) into a voltage pulse for subsequent display and processing. Note that the  $50\ \Omega$  resistors and  $47\ \text{nF}$  capacitors (A250 pins 4 and 11) shown in the figure, along with the  $300\ \text{M}\Omega$  resistor and  $1\ \text{pF}$  capacitor (A250 feedback loop), are internal to the A250 metal 14-pin dip package. The basic idea and advantages of a charge sensitive preamplifier are described in references 19 and 20. The high current gain factor of the field effect transistor (FET) reduces drift in the preamplifier output voltage caused by integration of the A250 operational amplifier input bias current by the feedback capacitor. As built (see Figure 21), the charge pulse amplifier circuit uses an Amptek PC250 test board for mounting the A250 preamplifier, with another circuit board to accommodate multiple FETs in parallel (if needed to more closely match the detector capacitance). The data shown in Figure 35 and Figure A-3 (described below) were obtained using a single 2SK152 FET.

The shaping circuit amplifies the pulses coming from the preamplifier and shapes them to avoid pulse overlap, or “pile-up.”<sup>19</sup> A Texas Instruments THS4031 broad-bandwidth, low-noise, high-speed amplifier is used for this purpose. The shaping is done by the differentiator ( $1.6\ \text{MHz}$  high-pass filter) and integrator ( $1.6\ \text{MHz}$  low-pass filter). The differentiator includes a  $3\ \text{M}\Omega$  resistor, in parallel with the  $100\ \text{pF}$  capacitor, that eliminates undershoot of the pulse tail (pole-zero cancellation). The  $13\ \text{MHz}$  low-pass filter,  $100\ \text{pF}$  feedback capacitor, and  $68\ \Omega$  output resistor shown in Figure A-1 are included to prevent amplifier feedback oscillations.

The sensitivity of the charge pulse amplifier circuit is demonstrated in Figure A-3, where the input is a long square pulse with a nominal amplitude of  $1.8\ \text{mV}$ . The input pulse length or period is much longer than  $10\ \mu\text{s}$ , so that only the leading edge of the pulse is evident in the figure. Note that the minimum expected amplitude of actual charge pulses coming from the Amptek A250 preamplifier is

8 mV (see Equation 6). This circuit can therefore detect pulses at least a factor of four smaller in amplitude than those expected when used with a FIND device as the detector.

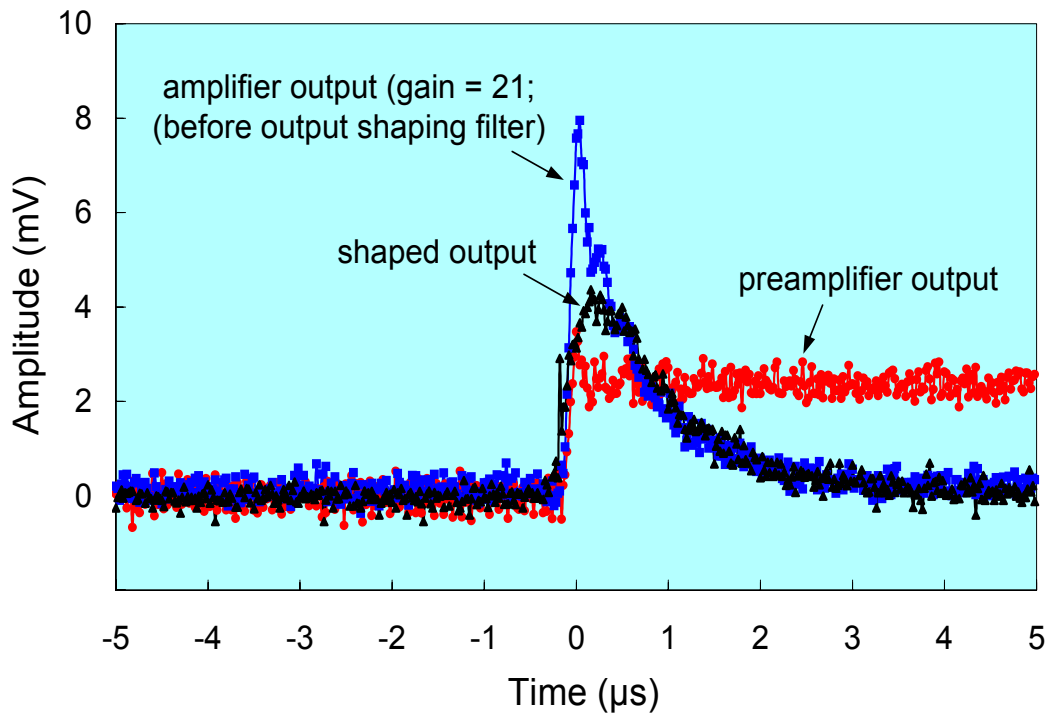


Figure A-3. Charge pulse amplifier circuit response to 1.8 mV square pulse input.







Approved for public release; distribution is unlimited.